Abstracta

Ano XXII - N. 06

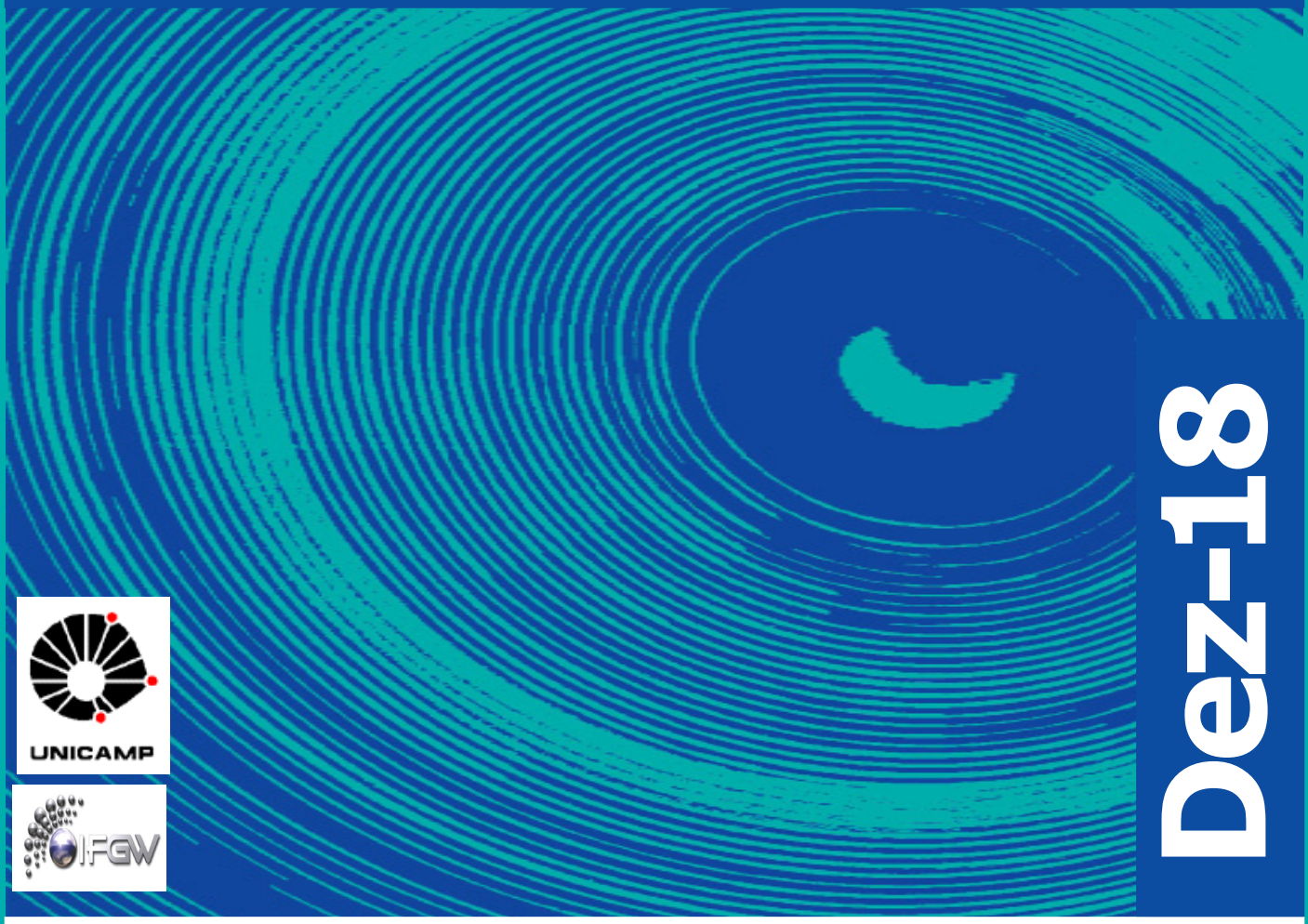

Dez-18

UNICAMP

IFGW

Artigos publicados - P364-2018 à P456-2018

Eventos publicados - P457-2018 à P459-2018

Artigos aceitos para publicação - A001-2018

Correções - Co006-2018

Defesas de Dissertações do IFGW - D018-2018 à D020-2018

Defesas de Teses do IFGW - T018-2018 à T019-2018

Defesas de Dissertações e Teses do PECIM - Pe004 à Pe005-2018

Artigos publicados

[P364-2018] "3D Printed Hollow-Core Terahertz Fibers"

Cruz, A. L. S.; **Cordeiro, C. M. B.***; Franco, M. A. R.

This paper reviews the subject of 3D printed hollow-core fibers for the propagation of terahertz (THz) waves. Several hollow and microstructured core fibers have been proposed in the literature as candidates for low-loss terahertz guidance. In this review, we focus on 3D printed hollow-core fibers with designs that cannot be easily created by conventional fiber fabrication techniques. We first review the fibers according to their guiding mechanism: photonic bandgap, antiresonant effect, and Bragg effect. We then present the modeling, fabrication, and characterization of a 3D printed Bragg and two antiresonant fibers, highlighting the advantages of using 3D printers as a path to make the fabrication of complex 3D fiber structures fast and cost-effective.

FIBERS 6[3], 43, 2018, DOI: 10.3390/fib6030043

[P365-2018] "A catalogue of structural and morphological measurements for DES Y1"

Tarsitano, E.; Hartley, W. G.; Amara, A.; **Sobreira, F.***; et al. DES Collaboration

We present a structural and morphological catalogue for 45 million objects selected from the first year data of the Dark Energy Survey (DES). Single Sersic fits and non-parametric measurements are produced for g, r, and i filters. The parameters from the best-fitting Sersic model (total magnitude, half-light radius, Sersic index, axis ratio, and position angle) are measured with GALFIT; the non-parametric coefficients (concentration, asymmetry, dumpiness, Gini, M20) are provided using the Zurich Estimator of Structural Types (ZEST+). To study the statistical uncertainties, we consider a sample of state-of-the-art image simulations with a realistic distribution in the input parameter space and then process and analyse them as we do with real data: this enables us to quantify the observational biases due to PSF blurring and magnitude effects and correct the measurements as a function of magnitude, galaxy size, Sersic index (concentration for the analysis of the non-parametric measurements) and ellipticity. We present the largest structural catalogue to date: we find that accurate and complete measurements for all the structural parameters are typically obtained for galaxies with SEXTRACTOR MAG_AUTO_I <= 21. Indeed, the parameters in the filters i and r can be overall well recovered up to MAG_AUTO <= 21.5, corresponding to a fitting completeness of similar to 90 per cent below this threshold, for a total of 25 million galaxies. The combination of parametric and non-parametric structural measurements makes this catalogue an important instrument to explore and understand how galaxies form and evolve. The catalogue described in this paper will be publicly released alongside the DES collaboration Y1 cosmology data products at the following URL: https://des.ncsa.illinois.edu/releases.

MONTHLY NOTICES OF THE ROYAL ASTRONOMICAL SOCIETY 481[2], 2018-2040, 2018. DOI: 10.1093/mnras/sty1970

[P366-2018] "About the influence of the density profile on neutron star cooling by neutrino emission"

Alvarez-Salazar, C. E.*; Quimbay, C. J.

We analyzed the influence of the density profile on neutron star cooling by neutrino emission, considering four different equations of state. After interpolated density profiles are obtained from discrete data, we calculate numerically, as a function of the radial distance to the center of the star, the following quantities: the neutron and proton number densities, their Fermi momenta, the proton fractions and the neutrino emissivities for two models of neutron stars with masses 1.33M(circle dot) and 1.4M(circle dot). For a specific equation of state and considering the effects of the density profile, we calculate the neutrino and photon luminosities and the cooling curve for these two models, taking into account two different possibilities for their particle composition. The photon luminosities obtained are consistent with the measurements of the bolometric luminosities for isolated neutron stars with thermal emission presented in the literature. The cooling curves are in good agreement with empirical data for the surface temperatures observed in several neutron stars.

ASTROPARTICLE PHYSICS 103, 67-73, 2018. DOI: 10.1016/j.astropartphys.2018.07.007

[P367-2018] "Adaptive density matrix renormalization group for disordered systems"

Xavier, J. C.; Hoyos, J. A.; **Miranda, E.***

We propose a simple modification of the density matrix renormalization-group (DMRG) method in order to tackle strongly disordered quantum spin chains. Our proposal, akin to the idea of the adaptive time-dependent DMRG, enables us to reach larger system sizes in the strong disorder limit by avoiding most of the metastable configurations, which hinder the performance of the standard DMRG method. We benchmark our adaptive method by revisiting the random antiferromagnetic XXZ spin-1/2 chain for which we compute the random--singlet ground-state average spin-spin correlation functions and von Neumann entanglement entropy. We then apply our method to the bilinear-biquadratic random antiferromagnetic spin-1 chain tuned to the antiferromagnet and gapless highly symmetric SU(3) point. We find the new result that the mean correlation function decays algebraically with the same universal exponent phi = 2 as the spin-1/2 chain. We then perform numerical and analytical strong-disorder renormalization-group calculations, which confirm this finding and generalize it for any highly symmetric SU(N) random-singlet state.

PHYSICAL REVIEW B 98[19], 195115, 2018. DOI: 10.1103/PhysRevB.98.195115

[P368-2018] "An ab initio investigation for elastic and electronically inelastic electron scattering from para-benzoquinone"

da Costa, R. F.*; Ruivo, J. C.; **Kossoski, F.***; Varella, M. T. N.; Bettega, M. H. F.; Jones, D. B.; Brunger, M. J.; **Lima, M. A. P.***

We report the results of ab initio calculations for elastic scattering and also for excitation of individual electronic states of para-benzoquinone (pBQ) by the impact of low-energy electrons. The calculations for elastic scattering were performed with the Schwinger multichannel method implemented with pseudopotentials (SMCPP) in the static-exchange (SE) plus polarization (SEP) approximation for energies up to 50 eV. The assignments for the resonance spectrum obtained in this study are, in general, in good agreement with previous results available in the literature. For electronic excitation by electron impact, the SMCPP method with N energetically open electronic states (N-open), at either the static-exchange (N(open) ch-SE) or the static-exchange-plus-polarisation (N(open)ch--SEP) approximation, was employed to calculate the scattering amplitudes using a channel coupling scheme that ranges from the 1ch-SEP up to the 89ch-SE level of approximation, depending on the energy of interest. Integral cross sections (ICSs) and differential cross sections (DCSs) were obtained for incident electron energies lying between 15 eV and 50 eV. The study focuses on the influence of multichannel coupling effects for electronically inelastic processes, more specifically,

on how the number of excited states included in the open--channel space impacts upon the convergence of the cross sections at intermediate and higher energies. In particular, we found that the magnitude of DCS and ICS results for electronic excitation decreases as more channels are included in the calculations. To the best of our knowledge, there are no other experimental or theoretical ICS or DCS results for excitation into individual electronic states of pBQ available in the literature between 15 and 50 eV against which we might compare the present calculations. Published by AIP Publishing.

JOURNAL OF CHEMICAL PHYSICS 149[17], 174308, 2018. DOI: 10.1063/1.5050622

[P369-2018] "Anisotropic flow in Xe-Xe collisions at root s(NN)=5.44 TeV"

Acharya, S.; Acosta, F. T.; Adamova, D.; **Albuquerque, D. S. D.*; Chinellato, D. D.*; De Souza, R. D.*; Takahashi, J.***; et al.
ALICE Collaboration

The first measurements of anisotropic flow coefficients v(n) for mid-rapidity charged particles in Xe-Xe collisions at root s(NN)=5.44TeV are presented. Comparing these measurements to those from Pb-Pb collisions at root s(NN)=5.02 TeV, v(2) is found to be suppressed for mid-central collisions at the same centrality, and enhanced for central collisions. The values of v(3) are generally larger in Xe-Xe than in Pb-Pb at a given centrality. These observations are consistent with expectations from hydrodynamic predictions. When both v(2) and v(3) are divided by their corresponding eccentricities for a variety of initial state models, they generally scale with transverse density when comparing Xe-Xe and Pb-Pb, with some deviations observed in central Xe-Xe and Pb-Pb collisions. These results assist in placing strong constraints on both the initial state geometry and medium response for relativistic heavy-ion collisions.

PHYSICS LETTERS B 784, 82-95, 2018. DOI: 10.1016/j.physletb.2018.06.059

[P370-2018] "Anomalous transport of light at the phase transition to localization: strong dependence with incident angle"

Jimenez-Villar, E.; Xavier, M. C. S.; Wetter, N. U.; Mestre, V.; Martins, W. S.; Basso, G. F.; **Ermakov, V. A.*; Marques, F. C.***; de Sa, G. F.

There has been a growing interest in disordered optical media in recent years due to their potential applications in solar collectors, random lasers, light confinement, and other advanced photonic functions. This paper studies the transport of light for different incidence angles in a strongly disordered optical medium composed of core-shell TiO2@Silica nanoparticles suspended in an ethanol solution. A decrease of optical conductance and an increase of absorption near the input border are reported when the incidence angle increases. The specular reflection, measured for the photons that enter the sample, is lower than the effective internal reflection undergone by the coherently backscattered photons in the exact opposite direction, indicating a nonreciprocal propagation of light. This study represents a novel approach in order to understand the complex physics involved at the phase transition to localization.

PHOTONICS RESEARCH 6[10], 929-942, 2018. DOI: 10.1364/PRJ.6.000929

[P371-2018] "Azimuthally-differential pion femtoscopy relative to the third harmonic event plane in Pb-Pbcollisions at root(NN)-N-S=2.76TeV"

Acharya, S.; Acosta, F. T.; Adamova, D.; **Albuquerque, D. S. D.*; Chinellato, D. D.*; De Souza, R. D.*; Takahashi, J.***; et al.
ALICE Collaboration

Azimuthally-differential femtoscopic measurements, being sensitive to spatio-temporal characteristics of the source as well as to the collective velocity fields at freeze out, provide very important information on the nature and dynamics of the system evolution. While the HBT radii oscillations relative to the second harmonic event plane measured recently reflect mostly the spatial geometry of the source, model studies have shown that the HBT radii oscillations relative to the third harmonic event plane are predominantly defined by the velocity fields. In this Letter, we present the first results on azimuthally-differential pion femtoscopy relative to the third harmonic event plane as a function of the pion pair transverse momentum k(T) for different collision centralities in Pb-Pb collisions at root(NN)-N-S = 2.76TeV. We find that the R-side and R-out radii, which characterize the pion source size in the directions perpendicular and parallel to the pion transverse momentum, oscillate in phase relative to the third harmonic event plane, similar to the results from 3+1D hydrodynamical calculations. The observed radii oscillations unambiguously signal a collective expansion and anisotropy in the velocity fields. A comparison of the measured radii oscillations with the Blast-Wave model calculations indicate that the initial state triangularity is washedout at freeze out.

PHYSICS LETTERS B 785, 320-331, 2018. DOI: 10.1016/j.physletb.2018.06.042

[P372-2018] "BAO from angular clustering: optimization and mitigation of theoretical systematics"

Chan, K. C.; Crocce, M.; Ross, A. J.; **Sobreira, F.***; et al.
DES Collaboration

We study the methodology and potential theoretical systematics of measuring baryon acoustic oscillations (BAO) using the angular correlation functions in tomographic bins. We calibrate and optimize the pipeline for the Dark Energy Survey Year 1 data set using 1800 mocks. We compare the BAO fitting results obtained with three estimators: the Maximum Likelihood Estimator (MLE), Profile Likelihood, and Markov Chain Monte Carlo. The fit results from the MLE arc the least biased and their derived la error bar are closest to the Gaussian distribution value after removing the extreme mocks with non-detected BAO signal. We show that incorrect assumptions in constructing the template, such as mismatches from the cosmology of the mocks or the underlying photo-z errors, can lead to BAO angular shifts. We find that MLE is the method that best traces this systematic biases, allowing to recover the true angular distance values. In a real survey analysis, it may happen that the final data sample properties are slightly different from those of the mock catalogue. We show that the effect on the mock covariance due to the sample differences can be corrected with the help of the Gaussian covariance matrix or more effectively using the eigenmode expansion of the mock covariance. In the eigenmode expansion, the eigenmodes are provided by some proxy covariance matrix. The eigenmode expansion is significantly less susceptible to statistical fluctuations relative to the direct measurements of the covariance matrix because of the number of free parameters is substantially reduced.

MONTHLY NOTICES OF THE ROYAL ASTRONOMICAL SOCIETY 480[3], 3031-3051, 2018. DOI: 10.1093/mnras/sty2036

[P373-2018] "Charged-particle nuclear modification factors in XeXe collisions at root S-NN=5.44 TeV"

Sirunyan, A. M.; Tumasyan, A.; **Chinellato, J. A.*; Tonelli Manganote, E. J.***; et al.
CMS Collaboration

The differential yields of charged particles having pseudorapidity within vertical bar eta vertical bar < 1 are measured using xenon-xenon (XeXe) collisions at root S-NN = 5.44 TeV. The data, corresponding to an integrated luminosity of 3.42 mu b(-1), were collected in 2017 by the CMS experiment at the LHC. The yields are reported as functions of collision centrality and transverse momentum, pT, from 0.5 to 100 GeV. A previously reported pT spectrum from proton-proton collisions at root S = 5.02 TeV is used for comparison after correcting for the difference in center-of-mass energy. The nuclear modification factors using this reference, R-AA*, are constructed and compared to previous measurements and theoretical predictions. In head-on collisions, the R-AA* has a value of 0.17 in the pT range of 6-8 GeV, but increases to approximately 0.7 at 100 GeV. Above approximate to 6 GeV, the XeXe data show a notably smaller suppression than previous results for lead-lead (PbPb) collisions at root S-NN = 5.02 TeV when compared at the same centrality (i.e., the same fraction of total cross section). However, the XeXe suppression is slightly greater than that for PbPb in events having a similar number of participating nucleons.

JOURNAL OF HIGH ENERGY PHYSICS [10], 138, 2018. DOI: 10.1007/JHEP10(2018)138

[P374-2018] "Constraints on Sub-GeV Dark-Matter-Electron Scattering from the DarkSide-50 Experiment"

Agnes, P.; Albuquerque, I. F. M.; Alexander, T.; **Machado, A. A.*; Segreto, E.***; et al.
DarkSide Collaboration

We present new constraints on sub-GeV dark-matter particles scattering off electrons based on 6780.0 kg d of data collected with the DarkSide-50 dual-phase argon time projection chamber. This analysis uses electroluminescence signals due to ionized electrons extracted from the liquid argon target. The detector has a very high trigger probability for these signals, allowing for an analysis threshold of three extracted electrons, or approximately 0.05 keVee. We calculate the expected recoil spectra for dark matterelectron scattering in argon and, under the assumption of momentum-independent scattering, improve upon existing limits from XENON10 for dark--matter particles with masses between 30 and 100 MeV/c(2).

PHYSICAL REVIEW LETTERS 121[11], 111303, 2018. DOI: 10.1103/PhysRevLett.121.111303

[P375-2018] "Dark Energy Survey Year 1 Results: A Precise H-0 Estimate from DES Y1, BAO, and D/H Data"

Abbott, T. M. C.; Abdalla, F. B.; Annis, J.; **Sobreira, F.***; et al.
Dark Energy Survey South Pole Tele

We combine Dark Energy Survey Year 1 clustering and weak lensing data with baryon acoustic oscillations and Big Bang nucleosynthesis experiments to constrain the Hubble constant. Assuming a flat Lambda CDM model with minimal neutrino mass (Sigma m(v), = 0.06 eV), we find H-0 = 67.4(-1.2)(+1.1) km s(-1) Mpc(-1) (68 per cent CL). This result is completely independent of Hubble constant measurements based on the distance ladder, cosmic microwave background anisotropies (both temperature and polarization), and strong lensing constraints. There are now five data sets that: (a) have no shared observational systematics; and (b) each constrains the Hubble constant with fractional uncertainty at the few-per cent level. We compare these five independent estimates, and find that, as a set, the differences between them are significant at the 2.5 sigma level (chi(2)/dof = 24/11, probability to exceed = 1.1 per cent). Having set the threshold for consistency at 30 sigma we combine all five data sets to arrive at H-0 = 69.3(-0.6)(+0.4) km s(-1) Mpc(-1).

MONTHLY NOTICES OF THE ROYAL ASTRONOMICAL SOCIETY 480[3], 3879-3888, 2018. DOI: 10.1093/mnras/sty1939

[P376-2018] "Dark Energy Survey Year 1 Results: calibration of redMaGiC redshift distributions in DES and SDSS from cross-correlations"

Cawthon, R; Davis, C. ; Gatti, M.; Vielzeuf, P.; Elvin-Poole, J.; **Sobreira, F.***; et al.
DES Collaboration

We present calibrations of the redshift distributions of redMaGiC galaxies in the Dark Energy Survey Year 1 (DES Y1) and Sloan Digital Sky Survey (SDSS) DR8 data. These results determine the priors of the redshift distribution of redMaGiC galaxies, which were used for galaxy clustering measurements and as lenses for galaxy-galaxy lensing measurements in DES Y1 cosmological analyses. We empirically determine the bias in redMaGiC photometric redshift estimates using angular cross-correlations with Baryon Oscillation Spectroscopic Survey (BOSS) galaxies. For DES, we calibrate a single-parameter redshift bias in three photometric redshift bins: z is an element of [0.15, 0.3], [0.3,0.45], and [0.45,0.6]. Our best-fit results in each bin give photometric redshift biases of vertical bar Delta z vertical bar < 0.01. To further test the redMaGiC algorithm, we apply our calibration procedure to SDSS redMaGiC galaxies, where the statistical precision of the cross-correlation measurement is much higher due to a greater overlap with BOSS galaxies. For SDSS, we also find best-fit results of vertical bar Delta z vertical bar < 0.01. We compare our results to other analyses of redMaGiC photometric redshifts.

MONTHLY NOTICES OF THE ROYAL ASTRONOMICAL SOCIETY , 481[2], 2427-2443, 2018. DOI: 10.1093/mnras/sty2424

[P377-2018] "Dark Energy Survey Year 1 results: weak lensing shape catalogues"

Zuntz, J.; Sheldon, E.; Samuroff, S.; **Sobreira, F.***; et al.
DES Collaboration

We present two galaxy shape catalogues from the Dark Energy Survey Year 1 data set, covering 1500 deg(2) with a median redshift of 0.59. The catalogues cover two main fields: Stripe 82, and an area overlapping the South Pole Telescope survey region. We describe our data analysis process and in particular our shape measurement using two independent shear measurement pipelines, METACALIBRATION and IM3SHAPE. The METACALIBRATION catalogue uses a Gaussian model with an innovative internal calibration scheme, and was applied to riz bands, yielding 34.8M objects. The IM3SHAPE catalogue uses amaximum-likelihood bulge/disc model calibrated using simulations, and was applied to r-band data, yielding 21.9M objects. Both catalogues pass a suite of null tests that demonstrate their fitness for use in weak lensing science. We estimate the 1 sigma uncertainties in multiplicative shear calibration to be 0.013 and 0.025 for the METACALIBRATION and IM3SHAPE catalogues, respectively.

MONTHLY NOTICES OF THE ROYAL ASTRONOMICAL SOCIETY, 481[1], 1149-1182, 2018. DOI: 10.1093/mnras/sty2219

[P378-2018] "DarkSide-50 532-day dark matter search with low-radioactivity argon"

Agnes, P.; Albuquerque, I. F. M.; Alexander, T.; **Machado, A. A.*; Segreto, E.***; et al.
DarkSide Collaboration

The DarkSide-50 direct-detection dark matter experiment is a dual-phase argon time projection chamber operating at Laboratori Nazionali del Gran Sasso. This paper reports on the blind analysis of a (16 660 +/- 270) kg d exposure using a target of low--radioactivity argon extracted from underground sources. We find no events in the dark matter selection box and set a 90% C. L.

upper limit on the dark matter-nucleon spin-independent cross section of 1.14x10(-44) cm(2) (3.78x10(-44) cm(2), 3.43x10(-43) cm(2)) for a WIMP mass of 100 GeV/c(2) (1 TeV/c(2), 10 TeV/c(2)).

PHYSICAL REVIEW D 98[10], 102006, 2018. DOI: 10.1103/PhysRevD.98.102006

[P379-2018] "DES science portal: Computing photometric redshifts"

Gschwend, J.; Rossel, A. C.; **Sobreira, F.***; et al.

A significant challenge facing photometric surveys for cosmological purposes is the need to produce reliable redshift estimates. The estimation of photometric redshifts (photo-zs) has been consolidated as the standard strategy to bypass the high production costs and incompleteness of spectroscopic redshift samples. Training-based photo-z methods require the preparation of a high-quality list of spectroscopic redshifts, which needs to be constantly updated. The photo-z training, validation, and estimation must be performed in a consistent and reproducible way in order to accomplish the scientific requirements. To meet this purpose, we developed an integrated web--based data interface that not only provides the framework to carry out the above steps in a systematic way, enabling the ease testing and comparison of different algorithms, but also addresses the processing requirements by parallelizing the calculation in a transparent way for the user. This framework called the Science Portal (hereafter Portal) was developed in the context the Dark Energy Survey (DES) to facilitate scientific analysis. In this paper, we show how the Portal can provide a reliable environment to access vast datasets, provide validation algorithms and metrics, even in the case of multiple photo-zs methods. It is possible to maintain the provenance between the steps of a chain of workflows while ensuring reproducibility of the results. We illustrate how the Portal can be used to provide photo-z estimates using the DES first year (Y1A1) data. While the DES collaboration is still developing techniques to obtain more precise photo-zs, having a structured framework like the one presented here is critical for the systematic vetting of DES algorithmic improvements and the consistent production of photo-zs in future DES releases.

ASTRONOMY AND COMPUTING 25, 58-80, 2018. DOI: 10.1016/j.ascom.2018.08.008

[P380-2018] "DES Y1 Results: validating cosmological parameter estimation using simulated Dark Energy Surveys"

MacCrann, N.; DeRose, J.; Wechsler, R. H.; **Sobreira, F.***; et al.
DES Collaboration

We use mock galaxy survey simulations designed to resemble the Dark Energy Survey Year 1 (DES Y1) data to validate and inform cosmological parameter estimation. When similar analysis tools are applied to both simulations and real survey data, they provide powerful validation tests of the DES Y1 cosmological analyses presented in companion papers. We use two suites of galaxy simulations produced using different methods, which therefore provide independent tests of our cosmological parameter inference. The cosmological analysis we aim to validate is presented in DES Collaboration et al. (2017) and uses angular two-point correlation functions of galaxy number counts and weak lensing shear, as well as their cross-correlation, in multiple redshift bins. While our constraints depend on the specific set of simulated realisations available, for both suites of simulations we find that the input cosmology is consistent with the combined constraints from multiple simulated DES Y1 realizations in the Omega(m) - sigma(8) plane. For one of the suites, we are able to show with high confidence that any biases in the inferred S-8 = sigma(8)(Omega(m)/0.3)(0.5) and Omega(m) are smaller than the DES Y1 1 - sigma uncertainties. For the other suite, for which we have fewer realizations, we are unable to be this conclusive; we infer a roughly 60 per cent (70 per cent) probability that systematic bias in the recovered Omega(m) (S-8) is sub-dominant to the DES Y1 uncertainty. As cosmological analyses of this kind become increasingly more precise, validation of parameter inference using survey simulations will be essential to demonstrate robustness.

MONTHLY NOTICES OF THE ROYAL ASTRONOMICAL SOCIETY 480[4], 4614-4635, 2018. DOI: 10.1093/mnras/sty1899

[P381-2018] "Dielectron production in proton-proton collisions at root s=7 TeV"

Acharya, S.; Collaboration, A.; Acosta, F. T.; **Albuquerque, D. S. D.*; Chinellato, D. D.*; De Souza, R. D.*; Takahashi, J.***; et al.

The first measurement of e(+)e(-) pair production at mid-rapidity (vertical bar eta vertical bar(e) < 0.8) in pp collisions at root s = 7TeV with ALICE at the LHC is presented. The dielectron production is studied as a function of the invariant mass (m(ee)< 3.3 GeV/c(2)), the pair transverse momentum (p(T,ee) < 8 GeV/c), and the pair transverse impact parameter (DCA(ee)), i.e., the average distance of closest approach of the reconstructed electron and positron tracks to the collision vertex, normalised to its resolution. The results are compared with the expectations from a cocktail of known hadronic sources and are well described when PYTHIA is used to generate the heavy--flavour contributions. In the low-mass region (0.14 < m(ee) < 1.1 GeV/c(2)), prompt and non-prompt e(+)e(-) sources can be separated via the DCA(ee). In the intermediate-mass region (1.1 < m(ee) < 2.7 GeV/c(2)), a double-differential fit to the data in m(ee) and p(T,ee) and a fit of the DCA(ee) distribution allow the total cc and bb cross sections to be extracted. Two different event generators, PYTHIA and POWHEG, can reproduce the shape of the two-dimensional m(ee) and p(T,ee) spectra, as well as the shape , of the DCA(ee) distribution, reasonably well. However, differences in the c (c) over bar and b (b) over bar cross sections are observed when using the generators to extrapolate to full phase space. Finally, the ratio of inclusive to decay photons is studied via the measurement of virtual direct photons in the transverse-momentum range 1 < p(T) < 8 GeV/c. This is found to be unity within the statistical and systematic uncertainties and consistent with expectations from next-to-leading order perturbative quantum chromodynamic calculations.

JOURNAL OF HIGH ENERGY PHYSICS 9, 064, 2018. DOI: 10.1007/JHEP09(2018)064

[P382-2018] "Dynamical Analysis of Three Distant Trans--Neptunian Objects with Similar Orbits"

Khain, T.; Becker, J. C.; **Sobreira, F.***; et al.
DES Collaboration

This paper reports the discovery and orbital characterization of two extreme trans-Neptunian objects (ETNOs), 2016 QV(89) and 2016 QU(89) , which have orbits that appear similar to that of a previously known object, 2013 UH15. All three ETNOs have semimajor axes a approximate to 172 au and eccentricities e approximate to 0.77. The angular elements (i, w, Omega) vary by 6 degrees, 15 degrees, and 49 degrees, respectively, between the three objects. The two new objects add to the small number of TNOs currently known to have semimajor axes between 150 and 250 au, and they serve as an interesting dynamical laboratory to study the outer realm of our solar system. Using a large ensemble of numerical integrations, we find that the orbits are expected to reside in close proximity in the (a, e) phase plane for roughly 100 Myr before diffusing to more separated values. We find that an explanation for the orbital configuration of the bodies as a collision product is disfavored.

We then explore other scenarios that could influence their orbits. With aphelion distances over 300 au, the orbits of these ETNOs extend far beyond the classical Kuiper Belt and an order of magnitude beyond Neptune. As a result, their orbital dynamics can be affected by the proposed new solar system member, referred to as Planet Nine in this work. With perihelion distances of 35-40 au, these orbits are also influenced by resonant interactions with Neptune. A full assessment of any possible new solar system planets must thus take into account this emerging class of TNOs.

ASTRONOMICAL JOURNAL 156[6], 273, 2018. DOI: 10.3847/1538-3881/aaeb2a

[P383-2018] "Edge magnetization and spin transport in an SU(2)-symmetric Kitaev spin liquid"

de Carvalho, V. S.*; Freire, H.; **Miranda, E.***; Pereira, R. G.

We investigate the edge magnetism and the spin transport properties of an SU(2)-symmetric Kitaev spin liquid (KSL) model put forward by Yao and Lee [Phys. Rev. Lett. 107, 087205 (2011)] on the honeycomb lattice. In this model, the spin degrees of freedom fractionalize into a Z(2) static gauge field and three species of either gapless (Dirac) or gapped (chiral) Majorana fermionic excitations. We find that, when a magnetic field is applied on a zigzag edge, the Dirac KSL exhibits a nonlocal magnetization associated with the existence of zero-energy edge modes. The application of a spin bias V = mu(up arrow) - mu(down arrow) y at the interface of the spin system with a normal metal produces a spin current into the KSL, which depends as a power law on V, in the zero-temperature limit, for both Dirac and chiral KSLs, but with different exponents. Lastly, we study the longitudinal spin Seebeck effect, in which a spin current is driven by the combined action of a magnetic field perpendicular to the plane of the honeycomb lattice and a thermal gradient at the interface of the KSL with a metal. Our results suggest that edge magnetization and spin transport can be used to probe the existence of charge-neutral edge states in quantum spin liquids.

PHYSICAL REVIEW B 98[15], 155105, 2018. DOI: 10.1103/PhysRevB.98.155105

[P384-2018] "Evidence of Band-Edge Hole Levels Inversion in Spherical CuInS2 Quantum Dots"

Nagamine, G*; Nunciaroni, H. B.*; McDaniel, H.; Efros, A. L.; **Cruz, C. H. D.*; Padilha, L. A.***

CuInS2 (CIS) quantum dots (QDs) have emerged as one of the most promising candidates for application in a number of new technologies, mostly due to their metal-free composition and their unique optical properties. Among those, the large Stokes shift and the long-lived excited state are the most striking ones. Although these properties are important, the physical mechanism that originates them is still under debate. Here, we use two-photon absorption spectroscopy and ultrafast dynamics studies to investigate the physical origin of those phenomena. From the two-photon absorption spectroscopy, we observe yet another unique property of CIS QDs, a two-photon absorption transition below the one-photon absorption band edge, which has never been observed before for any other semiconductor nanostructure. This originates from the inversion of the IS and 1P hole level order at the top of the valence band and results in a blue-shift of the experimentally measured one photon absorption edge by nearly 100 to 200 meV. However, this shift is not large enough to account for the Stokes shift observed, 200-500 meV. Consequently, despite the existence of the below band gap optical transition, photoluminescence in CIS QDs must originate from trap sites. These conclusions are reinforced by the multiexciton dynamics studies. From those, we demonstrate that biexciton Auger recombination behaves similarly to negative trion dynamics on these nanomaterials, which suggests that the trap state is an electron donating site.

NANO LETTERS 18, 10, 6353-6359, 2018. DOI: 10.1021/acs.nanolett.8b02707

[P385-2018] "Extreme- and high-synchrotron-peaked blazars at the limit of Fermi-LAT detectability: the gamma-ray spectrum of 1BIGB sources"

Arsioli, B.*; de Almeida, U. B.; Prandini, E.; Fraga, B.; Foffano, L.

We present the 1-100 GeV spectral energy distribution (SED) for a population of 148 high-synchrotron-peaked (HSP) blazars recently detected with Fermi LAT as part of the First Brazil-ICRANet Gamma-ray Blazar (1BIGB) catalogue. Most of the 1BIGB sources have their gamma-ray spectral properties presented here for the first time, representing a significant new extension of the gamma-ray blazar population. Since our sample was originally selected from an excess signal in the 0.3-500 GeV band, the sources stand out as promising TeV blazar candidates, potentially in reach of the forthcoming very high energy (VHE) gamma-ray observatory, Cherenkov Telescope Array (CTA). The flux estimates presented here are derived considering PASS8 data, integrating over more than 9 yr of Fenni LAT observations. We also review the full broad--band fit between 0.3 and 500 GeV presented in the original 1BIGB paper for all sources, updating the power-law parameters with currently available Fermi LAT data set. The importance of these sources in the context of VHE population studies with both current instruments and the future CTA is evaluated. To do so, we select a subsample of 1BIGB sources and extrapolate their gamma-ray SEDs to the highest energies, properly accounting for absorption due to the extragalactic background light. We compare those extrapolations to the published CTA sensitivity curves and estimate their detectability by CTA. Two notable sources from our sample, namely 1BIGB J224910.6 - 130002 and 1BIGB J194356.2+211821, are discussed in greater detail. All gamma-ray SEDs are made publicly available via the Brazilian Science Data Center (BSDC) service, maintained at CBPF, in Rio de Janeiro.

MONTHLY NOTICES OF THE ROYAL ASTRONOMICAL SOCIETY 480[2], 2165-2177, 2018. DOI: 10.1093/mnras/sty1975

[P386-2018] "Flexible metal-free supercapacitors based on multilayer graphene electrodes"

Augusto, G. D.; Scarminio, J.; Silva, P. R. C.; **de Siervo, A.***; Rout, C. S.; **Rouxinol, F.***; Gelamo, R. V.

We report the development of flexible self-supported metal--free electrodes based on non-oxidized graphene multilayer (MLG) paper, utilized to assemble bendable electrochemical supercapacitors. Using a simplified production method various electrodes exhibiting high conductivity were prepared and its structural, morphological, chemical and electrical properties characterized. Measurements in supercapacitors assembled from MLG electrodes and PANI-coated MLG electrodes show excellent electrochemical characteristics, with specific capacitances of 58 mF cm(-2) and 451 F g(-1) with 84% and 103% of capacitance retention after 1000 cycles, respectively. The energy and power density obtained for the PANI/MLG flexible supercapacitor reached 17.0 Wh g(-1) and 3.61 kW kg(-1), respectively. Moreover, in bending tests, the supercapacitors displayed an excellent mechanical and electrochemical stability. As an important result of this study, MLG electrodes appear as an interesting material for flexible high performance energy storage devices.

ELECTROCHIMICA ACTA 285, 241-253, 2018. DOI: 10.1016/j.electacta.2018.07.223

[P387-2018] "Forecasts for warm dark matter from photometric galaxy surveys"

Martins, J.S.; Rosenfeld, R.; **Sobreira, F.***; et al.

We present a Fisher matrix forecast for the sensitivity on the mass of a thermal warm dark matter (WDM) particle from current (DES-like) and future (LSST-like) photometric galaxy surveys using the galaxy angular power spectrum. We model the non-linear clustering using a modified Halo Model proposed to account for WDM effects. We estimate that from this observable alone a lower bound of m(wdm) > 647 eV (m(wdm) > 126 eV) for the LSST (DES) case could be obtained.

MONTHLY NOTICES OF THE ROYAL ASTRONOMICAL SOCIETY 481[1], 1290-1299, 2018. DOI: 10.1093/mnras/sty2300

[P388-2018] "Forward elastic scattering and Pomeron models"

Broilo, M.; Luna, E. G. S.; **Menon, M. J.***

Recent data from LHC13 by the TOTEM Collaboration indicate an unexpected decrease in the value of the rho parameter and sigma(tot) value in agreement with the trend of previous measurements at 7 and 8 TeV. These data at 13 TeV are not simultaneously described by the predictions from Pomeron models selected by the COMPETE Collaboration but show agreement with the maximal Odderon dominance, as recently demonstrated by Martynov and Nicolescu. Here, we present a detailed analysis on the applicability of Pomeron dominance by means of a general class of forward scattering amplitude, consisting of even-under-crossing leading contributions associated with single, double, and triple poles in the complex angular momentum plane and subleading even and odd Regge contributions. The analytic connection between sigma(tot) and rho is obtained by means of singly subtracted dispersion relations, and we carry out fits to pp and (p) over barp data in the interval 5 GeV-13 TeV. The data set comprises all the accelerator data below 7 TeV, and we consider two independent ensembles by adding either only the TOTEM data or the TOTEM and ATLAS data at the LHC energy region. In the data reductions to each ensemble, the uncertainty regions are evaluated with both one and two standard deviations (similar to 68% and similar to 95% CL, respectively). Besides the general analytic model, we investigate four particular cases of interest, three of them typical of outstanding models in the literature. We conclude that, within the experimental and theoretical uncertainties and both ensembles, the general model and three particular cases are not able to describe the sigma(tot) and rho data at 13 TeV simultaneously. However, if the discrepancies between the TOTEM and ATLAS data are not resolved, one Pomeron model, associated with double and triple poles and with only 7 free parameters, seems not to be excluded by the complete set of experimental information presently available.

PHYSICAL REVIEW D 98[7], 074006, 2018. DOI: 10.1103/PhysRevD.98.074006

[P389-2018] "Gd3+ as a probing and tuning tool of strong electronic correlations in the heavy-fermion Kondo lattice compound YbFe2Zn20"

Cabrera-Baez, M.*; Avila, M. A.; **Rettori, C.***

We report on the magnetic, thermodynamic, and electronic properties of the Gd-doped Kondo-lattice compound YbFe2Zn20 (T-K approximate to 32 K) by means of T-dependent magnetization, specific heat, and electron spin resonance (ESR) measurements. As Gd is incorporated in this system (Yb1-xGdx Fe2Zn20), the Yb contribution to the Sommerfeld coefficient remains almost unaltered for x = 0.005 and 0.01 at gamma(eff) approximate to 500 mJ mol(-1) K-2, however, for x = 0.05, it is reduced to gamma(eff) = 450 mJ mol(-1) K-2. As expected for heavy-fermion systems, the Gd3+ ESR experiments show an enhanced Korringa relaxation rate, b = d(Delta H)/(dT), due to the exchange interaction between the Gd3+ localized magnetic moment and the high 4f-conduction electrons (ce) density of states at the Fermi level. Below T-K, the Gd3+ ESR g shift presents a peculiar T dependence. For x less than or similar to 0.01, we associate the g shift to an internal molecular AFM field due to the ce screening of the Yb3+ magnetic moments in the Kondo condensate with a value of lambda = -2.80(1) mol Oe/emu. The negative value reflects a singlet nonmagnetic ground-state formation, consistent with a Kondo-lattice system. Still below T-K, but for x = 0.05, the Gd3+ ESR g shift presents a positive T dependence, which we now associate to an internal molecular FM field due to a Gd3+-Gd3+ superexchangelike interaction via extended Fe 3d ce. A Fermi surface reconstruction process is found to take place in the crossover from the high-T to low-T regimes, such that a momentum transfer dependence of the Gd3+-ce exchange interaction [J(f--ce) (q)] in the former is lost as the Kondo condensate sets in.

PHYSICAL REVIEW B 98[16], 165106, 2018. DOI: 10.1103/PhysRevB.98.165106

[P390-2018] "Hydrated Excess Proton Raman Spectral Densities Probed in Floating Water Bridges"

Teschke, O.*; de Castro, R.*; Valente, J. F.*; Soares, D. M.*

Excess proton structures in water remain unclear. The motion and nature of excess protons in water were probed using a supported water bridge structure in electric field (E) with an intensity of similar to 10(6) Vim. The experimental setup generated protons that exhibit a long lifetime. The effect of excess protons in water induced a similar to 3% variation in the pH for a 300 V overvoltage at the cathode. The current versus voltage curves show a current space charge-limited operation. By measuring the space-charge distribution in both the cathode and anode and by adjusting the Mott-Gurney law to the measured excess hydrated proton current and the voltage in drope cationic space charge region, the protonic mobility was determined to be similar to 200 x 10(-8) m(2)/(V.s) (E approximate to 4 x 10(6) V/m). This measured mobility, which is typically five times larger than the reported mobility for protons in water, is in agreement with the mechanism outlined by Grotthuss in 1805. The measured mid-Raman spectrum covering 1000-3800 cm(-1) range indicates the species character. The hydrated excess proton spectral response through the mid-Raman at 1760 and 3200 cm(-1) was attributed to the Zundel complex and the region at similar to 2000 to similar to 2600 cm(-1) response is attributed to the Eigen complex, indicating a core structure simultaneously with a Eigen-like and Zundel-like character, suggesting a rapid fluctuation between these two structures or a new specie.

ACS OMEGA 3[10], 13977-13983, 2018. DOI: 10.1021/acsomega.8b02285

[P391-2018] "Impact of disorder on the superconducting transition temperature near a Lifshitz transition"

Trevisan, T. V.*; Schutt, M.; Fernandes, R. M.

Multiband superconductivity is realized in a plethora of systems, from high-temperature superconductors to very diluted superconductors. While several properties of multiband superconductors can be understood as straightforward generalizations of their single-band counterparts, recent works have unveiled rather unusual behaviors unique to the former case. In this regard, a regime that has received significant attention is that near a Lifshitz transition, in which one of the bands crosses the Fermi level.

In this paper, we investigate how impurity scattering tau(-1) affects the superconducting transition temperature T-c across a Lifshitz transition, in the regime where intraband pairing is dominant and interband pairing is subleading. This is accomplished by deriving analytic asymptotic expressions for T-c and partial derivative T-c/partial derivative tau(-1) in a two--dimensional two-band system. When the interband pairing interaction is repulsive, we find that, despite the incipient nature of the band crossing the Fermi level, interband impurity scattering is extremely effective in breaking Cooper pairs, making partial derivative T-c/partial derivative tau(-1) quickly approach the limiting Abrikosov-Gor'kov value of the high-density regime. In contrast, when the interband pairing interaction is attractive, pair-breaking is much less efficient, affecting T-c only mildly at the vicinity of the Lifshitz transition. The consequence of this general result is that the behavior of T-c across a Lifshitz transition can be qualitatively changed in the presence of strong enough disorder: Instead of displaying a sharp increase across the Lifshitz transition, as in the clean case, T-c can actually display a maximum and be suppressed at the Lifshitz transition. These results shed light on the nontrivial role of impurity scattering in multiband superconductors.

PHYSICAL REVIEW B 98[9], 094514, 2018. DOI: 10.1103/PhysRevB.98.094514

[P392-2018] "In-situ monitoring by thermal lens microscopy of a photocatalytic reduction process of hexavalent chromium"

Cedeno, E.*; Plazas-Saldana, J.; Gordillo-Delgado, F.; Bedoya, A.; Marin, E.

In this work, we describe the application of a micro-spatial thermal lens spectroscopy setup (thermal lens microscope, TLM) with coaxial counter-propagating pump, and probe laser beams, and an integrated passive optical Fabry-Perot, to quantify the Cr-VI concentration in water during a photocatalytic reaction in-situ. A series of test samples was analyzed using the 1.5 diphenil carbazide colorimetric method. A calibration curve was obtained by plotting of the TLM signal as a function of the concentration of Cr(VI) in a range between 0 and 10 mu g/L (1 mu g/L = 1 ppb, part per billion), with a detection limit of 53 ng/L (1 ng/L = 1 ppt, part per trillion). A solution of 10 mu g/L Cr(VI) in distillated water was placed into a cell in contact with an iron-incorporated titanium dioxide film, which was previously grown onto a 1 mm thick glass microscope slide by the sol-gel dip-coating technique. The TLM signal was registered as a function of the photocatalysis time measured from the beginning of the process, radiating the film with UV--violet light. The Cr(VI) concentration was determined with the calibration curve and after the first 50 minutes a reduction of 95 % of Cr(VI) was observed, being the chemical reaction kinetic described by a potential time decreasing function.

REVISTA MEXICANA DE FISICA 64[5], 507-511, 2018. DOI: 10.31349/RevMexFis.64.507

[P393-2018] "Inclusive J/psi production in Xe-Xe collisions at root s(NN)=5.44 TeV"

Acharya, S.; Acosta, F. T.; Adamova, D.; **Albuquerque, D. S. D.*; Chinellato, D. D.*; De Souza, R. D.*; Takahashi, J.***; et al.
ALICE Collaboration

Inclusive J/psi production is studied in Xe-Xeinteractions at a centre-of-mass energy per nucleon pair of root s(NN) = 5.44 TeV, using the ALICE detector at the CERN LHC. The J/psi meson is reconstructed via its decay into a muon pair, in the centre-of-mass rapidity interval 2.5 < y < 4 and down to zero transverse momentum. In this Letter, the nuclear modification factors R-AA for inclusive J/psi, measured in the centrality range 0-90% as well as in the centrality intervals 0-20% and 20-90% are presented. The R-AA values are compared to previously published results for Pb-Pbcollisions at root s(NN) = 5.02 TeV and to the calculation of a transport model. A good agreement is found between Xe--Xe and Pb-Pbresults as well as between data and the model.

PHYSICS LETTERS B 785, 419-428, 2018. DOI: 10.1016/j.physletb.2018.08.047

[P394-2018] "Large-scale Cosmic-Ray Anisotropies above 4 EeV Measured by the Pierre Auger Observatory"

Aab, A.; Abreu, P.; Aglietta, M.; Albuquerque, I. F. M.; **Chinellato, J. A.*; Daniel, B.*; Diaz Castro, M. L.*; Dobrigkeit, C.*; Fauth, A. C.*; Muller, M. A.*; Pereira, L. A. S.***; et al.
Pierre Auger Collaboration

We present a detailed study of the large-scale anisotropies of cosmic rays with energies above 4 EeV measured using the Pierre Auger Observatory. For the energy bins [4, 8] EeV and E >= 8 EeV, the most significant signal is a dipolar modulation in R.A. at energies above 8 EeV, as previously reported. In this paper we further scrutinize the highest-energy bin by splitting it into three energy ranges. We find that the amplitude of the dipole increases with energy above 4 EeV. The growth can be fitted with a power law with index beta = 0.79 +/- 0.19. The directions of the dipoles are consistent with an extragalactic origin of these anisotropies at all the energies considered. Additionally, we have estimated the quadrupolar components of the anisotropy: they are not statistically significant. We discuss the results in the context of the predictions from different models for the distribution of ultrahigh-energy sources and cosmic magnetic fields.

ASTROPHYSICAL JOURNAL 868[1], 4, 2018. DOI: 10.3847/1538-4357/aae689

[P395-2018] "Measurement of D-0, D+, D*+ and D-s(+) production in Pb-Pb collisions at root s(NN)=5:02 TeV"

Acharya, S.; Acosta, F. T.; Adamova, D.; **Albuquerque, D. S. D.*; Chinellato, D. D.*; De Souza, R. D.*; Takahashi, J.***; et al.
ALICE Collaboration

We report measurements of the production of prompt D-0, D+, D*+ and D TeV. For D mesons, the values of R-AA are larger than those of non-strange D mesons, but compatible within uncertainties. In central collisions the average R-AA of non-strange D mesons is compatible with that of charged particles for p 8 GeV/c, while it is larger at lower p(T). The nuclear modification factors for strange and non--strange D mesons are also compared to theoretical models with different implementations of in-medium energy loss.

JOURNAL OF HIGH ENERGY PHYSICS [10], 2018. DOI: 10.1007/JHEP10(2018)174

[P396-2018] "Measurement of the groomed jet mass in PbPb and pp collisions at root s(NN)=5:02 TeV"

Sirunyan, A. M.; Tumasyan, A.; Adam, W.**; Chinellato, J. A.*; Tonelli Manganote, E. J.***; et al.
CMS Collaboration

A measurement of the groomed jet mass in PbPb and pp collisions at a nucleon-nucleon center-of-mass energy of 5.02 TeV with the CMS detector at the LHC is presented.

Jet grooming is a recursive procedure which sequentially removes soft constituents of a jet until a pair of hard subjets is found. The resulting groomed jets can be used to study modifications to the parton shower evolution in the presence of the hot and dense medium created in heavy ion collisions. Predictions of groomed jet properties from the pythia and herwig++ event generators agree with the measurements in pp collisions. When comparing the results from the most central PbPb collisions to pp data, a hint of an increase of jets with large jet mass is observed, which could originate from additional medium-induced radiation at a large angle from the jet axis. However, no modification of the groomed mass of the core of the jet is observed for all PbPb centrality classes. The PbPb results are also compared to predictions from the jewel and q-pythia event generators, which predict a large modification of the groomed mass not observed in the data.

JOURNAL OF HIGH ENERGY PHYSICS 10[161], 2018. DOI: 10.1007/JHEP10(2018)161

[P397-2018] "Measurement of the production cross section for single top quarks at root s=13 TeV"

Sirunyan, A. M.; Tumasyan, A.; **Chinellato, J. A.*; Tonelli Manganote, E. J.***; et al.
CMS Collaboration

A measurement is presented of the associated production of a single top quark and a W boson in proton -proton collisions at root s = 13 TeV by the CMS Collaboration at the CERN LHC. The data collected corresponds to an integrated luminosity of 35.9 fb(-1). The measurement is performed using events with one electron and one muon in the final state along with at least one jet originated from a bottom quark. A multivariate discriminant, exploiting the kinematic properties of the events, is used to separate the signal from the dominant tt background. The measured cross section of 63.1 +/- 1.8(stat) +/- 6.4(syst) +/- 2.1 (lumi) pb is in agreement with the standard model expectation.

JOURNAL OF HIGH ENERGY PHYSICS [10], 117, 2018. DOI: 10.1007/JHEP10(2018)117

[P398-2018] "Measurements of low-p(T) electrons from semileptonic heavy-flavour hadron decays at mid-rapidity in pp and Pb-Pb collisions at root s(NN)=2.A76 TeV"

Acharya, S.; Acosta, F. T.; Adamova, D.; **Albuquerque, D. S. D.*; Chinellato, D. D.*; De Souza, R. D.*; Takahashi, J.***; et al.
ALICE Collaboration

Transverse-momentum (p(T)) differential yields of electrons from semileptonic heavy-flavour hadron decays have been measured in the most central (0-10%) and in semi-central (20-40%) Pb-Pb collisions at TeV. The corresponding production cross section in pp collisions has been measured at the same energy with substantially reduced systematic uncertainties with respect to previously published results. The modification of the yield in Pb-Pb collisions with respect to the expectation from an incoherent superposition of nucleon-nucleon collisions is quantified at mid-rapidity (|y| < 0.8) in the p(T) interval 0.5-3 GeV/c via the nuclear modification factor, R-AA. This paper extends the p(T) reach of the R-AA measurement towards significantly lower values with respect to a previous publication. In Pb-Pb collisions the p(T)-differential measurements of yields at low p(T) are essential to investigate the scaling of heavy--flavour production with the number of binary nucleon-nucleon collisions. Heavy-quark hadronization, a collective expansion and even initial-state effects, such as the nuclear modification of the Parton Distribution Function, are also expected to have a significant effect on the measured distribution.

JOURNAL OF HIGH ENERGY PHYSICS [10], 061, 2018. DOI: 10.1007/JHEP10(2018)061

[P399-2018] "Measurements of the differential jet cross section as a function of the jet mass in dijet events from proton -proton collisions at=13 TeV"

Sirunyan, A. M.; Tumasyan, A.; Adam, W.; **Chinellato, J. A.*; Tonelli Manganote, E. J.***; et al
CMS Collaboration

Measurements of the differential jet cross section are presented as a function of the jet mass in dijet events, in bins of jet transverse momentum, with and without a jet grooming algorithm. The data have been recorded by the CMS Collaboration in proton-proton collisions at the LHC at a center-of-mass energy of 13 TeV and correspond to an integrated luminosity of 2.3 fb(-1). The absolute cross sections show slightly different jet transverse momentum spectra in data and Monte Carlo event generators for the settings used. Removing this transverse momentum dependence, the normalized cross section for ungroomed jets is consistent with the prediction from Monte Carlo event generators for masses below 30% of the transverse momentum. The normalized cross section for groomed jets is measured with higher precision than the ungroomed cross section. Semi-analytical calculations of the jet mass beyond leading logarithmic accuracy are compared to data, as well as predictions at leading order and next-to-leading order, which include parton showering and hadronization. Overall, in the normalized cross section, the theoretical predictions agree with the measured cross sections within the uncertainties for masses from 10 to 30% of the jet transverse momentum.

JOURNAL OF HIGH ENERGY PHYSICS [11], 113, 2018. DOI: 10.1007/JHEP11(2018)113

[P400-2018] "Medium modification of the shape of small-radius jets in central Pb-Pb collisions at root s(NN)=2:76 TeV"

Acharya, S.; Acosta, F. T.; **Albuquerque, D. S. D.*; Chinellato, D. D.*; De Souza, R. D.*; Takahashi, J.***; et al.
The ALICE collaboration

We present the measurement of a new set of jet shape observables for trackbased jets in central Pb-Pb collisions at p sNN = 2 : 76TeV. The set of jet shapes includes the fi rst radial moment or angularity, g; the momentum dispersion, pTD; and the di ff erence between the leading and sub-leading constituent track transverse momentum, LeSub. These observables provide complementary information on the jet fragmentation and can constrain di ff erent aspects of the theoretical description of jet-medium interactions. The jet shapes were measured for a small resolution parameter R = 0 : 2 and were fully corrected to particle level. The observed jet shape modi fi cations indicate that in-medium fragmentation is harder and more collimated than vacuum fragmentation as obtained by PYTHIA calculations, which were validated with the measurements of the jet shapes in proton-proton collisions at p s = 7TeV. The comparison of the measured distributions to templates for quark and gluon-initiated jets indicates that in-medium fragmentation resembles that of quark jets in vacuum. We further argue that the observed modi fi cations are not consistent with a totally coherent energy loss picture where the jet loses energy as a single colour charge, suggesting that the medium resolves the jet structure at the angular scales probed by our measurements (R = 0 : 2). Furthermore, we observe that small-R jets can help to isolate purely energy loss e ff ects from other e ff ects that contribute to the modi fi cations of the jet shower in medium such as the correlated background or medium response.

JOURNAL OF HIGH ENERGY PHYSICS [10], 139, 2018. DOI: 10.1007/JHEP10(2018)139

[P401-2018] "Minimal dissipation in processes far from equilibrium"

Bonanca, M. V. S.*; Deffner, S.

A central goal of thermodynamics is to identify optimal processes during which the least amount of energy is dissipated into the environment. Generally, even for simple systems, such as the parametric harmonic oscillator, optimal control strategies are mathematically involved and contain peculiar and counterintuitive features. We show that optimal driving protocols determined by means of linear-response theory exhibit the same step and delta-peak-like structures that were previously found from solving the full optimal control problem. However, our method is significantly less involved, since only a minimum of a quadratic form has to be determined. In addition, our findings suggest that optimal protocols from linear-response theory are applicable far outside their actual range of validity.

PHYSICAL REVIEW E 98[4], 042103, 2018. DOI: 10.1103/PhysRevE.98.042103

[P402-2018] "Modelling the Tucana III stream - a close passage with the LMC"

Erkal, D.; Li, T. S.; **Sobreira, F.***; et al.

We present results of the first dynamical stream fits to the recently discovered Tucana III stream. These fits assume a fixed Milky Way potential and give proper motion predictions, which can be tested with the upcoming Gaia Data Release 2 (DR2). These fits reveal that Tucana III is on an eccentric orbit around the Milky Way and, more interestingly, that Tucana III passed within 15 kpc of the Large Magellanic Cloud (LMC) approximately 75 Myr ago. Given this close passage, we fit the Tucana III stream in the combined presence of the Milky Way and the LMC. We find that the predicted proper motions depend on the assumed mass of the LMC and that the LMC can induce a substantial proper motion perpendicular to the stream track. A detection of this misalignment will directly probe the extent of the LMC's influence on our Galaxy, and has implications for nearly all methods which attempt to constraint the Milky Way potential. Such a measurement will be possible with the upcoming Gaia DR2, allowing for a measurement of the LMC's mass.

MONTHLY NOTICES OF THE ROYAL ASTRONOMICAL SOCIETY 481[3], 3148-3159, 2018. DOI: 10.1093/mnras/sty2518

[P403-2018] "Molecular organization relationship of low--bandgap polymers at the air water interface and in solid films"

de Oliveira, V. J. R.; da Silva, E. A.; **Braunger, M. L.***; Awada, H.; de Santana, H.; Hiorns, R. C.; Lartigau-Dagron, C.; Olivati, C. D.

Low-bandgap organic polymers, poly((4,4 bis(2 ethylhexyl) cyclopenta [2,1 b:3,4 b']dithiophene) 2,6 diyl al (2,1,3 benzothiadiazole) 4,7 diyl(PCPDTBT), and poly [(4,4' dioctyldithieno[3,2 b:2',3'd] silol 2,6 diyl) alt (2,1,3 benzothiadiazole) 4,7 diyl)], (Si-PCPDTBT) were analyzed at the air-water interface forming a Langmuir monolayer. In order to form stable monolayers and to transfer to solid supports, amphiphilic molecules of stearic acid (SA) were mixed with them. For the pristine polymers, the floating monolayers were transferred onto solid substrates via the Langmuir-Schaefer (LS) technique. Surface pressure-area isotherms and compressibility modulus curves demonstrated that the SA incorporation to the polymers at the air-water interface modified the rheological properties of the Langmuir films, since the films became less compressible at higher pressures and there is clear conformational reorganization taking place at intermediary pressures. The UV-Vis absorption also depicted the changes on the overall film morphology by the shift on the maximum absorption bands, and along with cyclic voltammetry curves the absorption spectra made it possible to estimate the energy diagrams for the polymers. Photoconductivity effects were observed for all the sample, among which the pristine polymersfabricated by LS showed better results, suggesting that the organization provided by the Langmuir-Blodgett (LB) technique was not enough to overcome the insulating Lharacteristic-olthe-SA molecules in this specific configuration.

JOURNAL OF MOLECULAR LIQUIDS 268, 114-121, 2018. DOI: 10.1016/j.molliq.2018.07.018

[P404-2018] "Nano-fried-eggs: Structural, optical, and magnetic characterization of physically prepared iron-silver nanoparticles"

Ramade, J.; Troc, N.; Boisron, O. ; Pellarin, M; Lebault, M. A.; Cottancin, E.; **Oiko, V. T. A.*; Gomes, R. C.*; Rodrigues, V.*; Hillenkamp, M.***

The prospect of combining both magnetic and plasmonic properties in a single nanoparticle promises both valuable insights on the properties of such systems from a fundamental viewpoint and numerous possibilities for technological applications. However, the combination of two of the most prominent metallic candidatesiron and silverhas presented numerous experimental difficulties because their thermodynamic properties impede miscibility and even coalescence. Herein, we present the thorough characterization of physically prepared Fe50Ag50 nanoparticles embedded in carbon and silica matrices via electron microscopy, optical spectroscopy, magnetometry and synchrotron-based X-ray spectroscopy. Iron and silver segregate completely into structures resembling fried eggs, with a nearly spherical, crystallized silver part surrounded by an amorphous structure of iron carbide or oxide, depending on the environment of the particles. Consequently, the particles exhibit both plasmonic absorption corresponding to the silver nanospheres in an oxide environment and a reduced but measurable magnetic response. The suitability of such nanoparticles for technological applications is discussed from the viewpoint of their high chemical reactivity with their environment.

NANO RESEARCH 11[11], 6074-6085, 2018. DOI: 10.1007/s12274-018-2125-6

[P405-2018] "Nanoclusters of crystallographically aligned nanoparticles for magnetic thermotherapy: aqueous ferrofluid, agarose phantoms and ex vivo melanoma tumour assessment"

Coral, D. F.; Soto, P. A.; Blank, V.; Veiga, A.; Spinelli, E.; Gonzalez, S.; Saracco, G. P.; Bab, M. A.; **Muraca, D.***; Setton-Avruj, P. C.; Roig, A.; Roguin, L.; Fernandez van Raap, M. B.

Magnetic hyperthermia is an oncological therapy where magnetic nanostructures, under a radiofrequency field, act as heat transducers increasing tumour temperature and killing cancerous cells. Nanostructure heating efficiency depends both on the field conditions and on the nanostructure properties and mobility inside the tumour. Such nanostructures are often incorrectly bench-marketed in the colloidal state and using field settings far off from the recommended therapeutic values. Here, we prepared nanoclusters composed of iron oxide magnetite nanoparticles crystallographically aligned and their specific absorption rate (SAR) values were calorimetrically determined in physiological fluids, agarose-gel-phantoms and ex vivo tumours extracted from mice challenged with B16-F0 melanoma cells. A portable, multipurpose applicator using medical field settings; 100 kHz and 9.3 kA m(-1), was developed and the results were fully analysed in terms of nanoclusters' structural and magnetic properties. A careful evaluation of the nanoclusters' heating capacity in the three milieus clearly indicates that the SAR values of fluid suspensions or agarose--gel-phantoms are not adequate to predict the real tissue temperature increase or the dosage needed to heat a tumour.

Our results show that besides nanostructure mobility, perfusion and local thermoregulation, the nanostructure distribution inside the tumour plays a key role in effective heating. A suppression of the magnetic material effective heating efficiency appears in tumour tissue. In fact, dosage had to be increased considerably, from the SAR values predicted from fluid or agarose, to achieve the desired temperature increase. These results represent an important contribution towards the design of more efficient nanostructures and towards the clinical translation of hyperthermia.

NANOSCALE 10[45], 21262-21274, 2018. DOI: 10.1039/c8nr07453d

[P406-2018] "Nanoporous Silicon Composite as Potential System for Sustained Delivery of Florfenicol Drug"

Hernandez-Montelongo, J.*; Oria, L.; Cardenas, A. B.; Benito, N.; Romero-Saez, M.; Recio-Sanchez, G.

Nanostructured porous silicon (nPSi) is a nanostructured biomaterial which has received considerable attention in biomedical applications due to its biocompatibility, biodegradability, high surface area, and the ease to modify its surface chemistry. In the present work, nPSi composite microparticles are evaluated as potential drug delivery system. nPSi layers are formed by electrochemical etching of silicon wafers in hydrofluoric acid solutions. This fabrication process allows modifying the main properties of nPSi layers, including the porosity, average pore size and pore shape, by simply controlling the main parameters in the process, such as the applied current density and the electrolyte composition. nPSi microparticles are prepared from the removal and fracture by ultrasound sonication of nPSi layers. Composites are obtained from oxidized nPSi (nPSi-Ox) microparticles cascade processed with chitosan (CHI) and -cyclodextrin (CD) biopolymers. Samples are evaluated as drug delivery system using florfenicol (FF) as model drug, due to its economical and sanitary importance in salmon industry. Drug loaded and release kinetic tests are performed in different media: distilled water and simulated seawater. Initial data show that nPSi-CD composites allow a mayor control in the drug time release kinetic compared to nPSi-Ox microparticles.

PHYSICA STATUS SOLIDI B-BASIC SOLID STATE PHYSICS 255, 10, 1700626, 2018. DOI: 10.1002/pssb.201700626

[P407-2018] "Neutral pion and eta meson production at midrapidity in Pb-Pb collisions at root S-NN=2.76 TeV"

Acharya, S.; Acosta, F. T.; Adamova, D.; **Albuquerque, D. S. D.*; Chinellato, D. D.*; De Souza, R. D.*; Takahashi, J.***; et al.
ALICE Collaboration

Neutral pion and eta meson production in the transverse momentum range 1 < p(T) < 20 GeV/c have been measured at midrapidity by the ALICE experiment at the Large Hadron Collider (LHC) in central and semicentral Pb-Pb collisions at root S-NN = 2.76 TeV. These results were obtained using the photon conversion method as well as the Photon Spectrometer (PHOS) and Electromagnetic Calorimeter detectors. The results extend the upper p(T) reach of the previous ALICE pi(0) measurements from 12 to 20 GeV/c and present the first measurement of eta meson production in heavy-ion collisions at the LHC. The eta/pi(0) ratio is similar for the two centralities and reaches at high p(T) a plateau value of 0.457 +/- 0.013(stat) +/- 0.018(syst) A suppression of similar magnitude for pi(0) and eta meson production is observed in Pb-Pb collisions with respect to their production in pp collisions scaled by the number of binary nucleon-nucleon collisions. We discuss the results in terms of Next to Leading Order (NLO) pQCD predictions and hydrodynamic models. The measurements show a stronger suppression than observed at lower center-of-mass energies in the p T range 6 < p(T) < 10 GeV/c. For p(T) < 3 GeV/c, hadronization models describe the pi(0) results while for the eta some tension is observed.

PHYSICAL REVIEW C 98[4], 044901, 2018. DOI: 10.1103/PhysRevC.98.044901

[P408-2018] "Non-ergodic states induced by impurity levels in quantum spin chains"

Rodriguez, A. O. G.*; Cabrera, G. G.*

The semi-infinite XY spin chain with an impurity at the boundary has been chosen as a prototype of interacting many--body systems to test for non-ergodic behavior. The model is exactly solvable in analytic way in the thermodynamic limit, where energy eigenstates and the spectrum are obtained in closed form. In addition of a continuous band, localized states may split off from the continuum, for some values of the impurity parameters. In the next step, after the preparation of an arbitrary non-equilibrium state, we observe the time evolution of the site magnetization. Relaxation properties are described by the long-time behavior, which is estimated using the stationary phase method. Absence of localized states defines an ergodic region in parameter space, where the system relaxes to a homogeneous magnetization. Out of this region, impurity levels split from the band, and localization phenomena may lead to non-ergodicity.

EUROPEAN PHYSICAL JOURNAL-SPECIAL TOPICS 227[3-4], SI, 301-311, 2018. DOI: 10.1140/epjst/e2018-00095-7

[P409-2018] "Nonresistive dissipative magnetohydrodynamics from the Boltzmann equation in the 14-moment approximation"

Denicol, G. S.; Huang, X. G.; Molnar, E.; **Monteiro, G. M.***; Niemi, H.; Noronha, J.; Rischke, D. H.; Wang, Q.

We derive the equations of motion of relativistic, nonresistive, second-order dissipative magnetohy-drodynamics from the Boltzmann equation using the method of moments. We assume the fluid to be composed of a single type of point--like particles with vanishing dipole moment or spin, so that the fluid has vanishing magnetization and polarization. In a first approximation, we assume the fluid to be nonresistive, which allows to express the electric field in terms of the magnetic field. We derive equations of motion for the irreducible moments of the deviation of the single-particle distribution function from local thermodynamical equilibrium. We analyze the Navier-Stokes limit of these equations, reproducing previous results for the structure of the first-order transport coefficients. Finally, we truncate the system of equations for the irreducible moments using the 14-moment approximation, deriving the equations of motion of relativistic, nonresistive, second-order dissipative magnetohydrodynamics. We also give expressions for the new transport coefficients appearing due to the coupling of the magnetic field to the dissipative quantities.

PHYSICAL REVIEW D 98[7], 076009, 2018. DOI: 10.1103/PhysRevD.98.076009

[P410-2018] "Novel etching protocol for epidote fission tracks"

Nakasuga, W. M.*; Saenz, C. A. T.; Curvo, E. A. C.; **Neto, J. C. H.*; Guedes, S.***; Resende, R. S.

Along the years, etching for fission tracks was a major issue in the development of the epidote fission track dating.

It was not a consensus in the scientific community. As an attempt to mitigate it, we present a novel etching protocol (HF 40% at 15 degrees C for 80 min) and test it in ten different natural samples etched with HF 40% at 15 degrees C for 80 min (nine epidotes and one clinozoisite). The samples had their chemical compositions determined, forming a database for epidote chemical compositions. Fission tracks were observed in five samples. The uranium content in the remaining four samples was too low and hence tracks could not be observed. Further analyses, Raman and uranium concentration, confirm this observation. Fission tracks were not observed in clinozoisite sample. The proposed etching protocol showed to be less hazardous and efficient to etching fission tracks in epidote.

RADIATION MEASUREMENTS 118, 26-30, 2018. DOI: 10.1016/j.radmeas.2018.08.007

[P411-2018] "Observation of Higgs Boson Decay to Bottom Quarks"

Sirunyan, A. M.; Tumasyan, A.; Adam, W.; **Chinellato, J. A.*; Tonelli Manganote, E. J.***; et al.
CMS Collaboration

The observation of the standard model (SM) Higgs boson decay to a pair of bottom quarks is presented. The main contribution to this result is from processes in which Higgs bosons arc produced in association with a W or Z boson (VH), and are searched for in final states including 0, 1, or 2 charged leptons and two identified bottom quark jets. The results from the measurement of these processes in a data sample recorded by the CMS experiment in 2017, comprising 41.3 fb(-1) of proton-proton collisions at root s = 13 TeV, are described. When combined with previous VH measurements using data collected at root s = 7, 8, and 13 TeV, an excess of events is observed at m(H) = 125 GeV with a significance of 4.8 standard deviations, where the expectation for the SM Higgs boson is 4.9. The corresponding measured signal strength is 1.01 +/- 0.22. The combination of this result with searches by the CMS experiment for H -> b (b) over bar in other production processes yields an observed (expected) significance of 5.6 (5.5) standard deviations and a signal strength of 1.04 +/- 0.20.

PHYSICAL REVIEW LETTERS 121[12], 121801, 2018. DOI: 10.1103/PhysRevLett.121.121801

[P412-2018] "Observation of inclined EeV air showers with the radio detector of the Pierre Auger Observatory"

Aab, A.; Abreu, P.; Aglietta, M.; **Chinellato, J. A.*; Daniel, B.*; Castro, M. L. Diaz*; Dobrigkeit, C.*; Fauth, A. C.*; Muller, M. A.*; Pereira, L. A. S.***; et al.
Pierre Auger Collaboration

With the Auger Engineering Radio Array (AERA) of the Pierre Auger Observatory, we have observed the radio emission from 561 extensive air showers with zenith angles between 60 degrees and 84 degrees. In contrast to air showers with more vertical incidence, these inclined air showers illuminate large ground areas of several km(2) with radio signals detectable in the 30 to 80 MHz band. A comparison of the measured radio--signal amplitudes with Monte Carlo simulations of a subset of 50 events for which we reconstruct the energy using the Auger surface detector shows agreement within the uncertainties of the current analysis. As expected for forward-beamed radio emission undergoing no significant absorption or scattering in the atmosphere, the area illuminated by radio signals grows with the zenith angle of the air shower. Inclined air showers with EeV energies are thus measurable with sparse radio-antenna arrays with grid sizes of a km or more. This is particularly attractive as radio detection provides direct access to the energy in the electromagnetic cascade of an air shower, which in case of inclined air showers is not accessible by arrays of particle detectors on the ground.

JOURNAL OF COSMOLOGY AND ASTROPARTICLE PHYSICS 10, 026, 2018. DOI: 10.1088/1475-7516/2018/10/026

[P413-2018] "Observation of the Z -> psi l(+)l(-) Decay in pp Collisions at root s=13 TeV"

Sirunyan, A. M.; Tumasyan, A.; Adam, W; **Chinellato, J. A.*; Tonelli Manganote, E. J.***; et al.
CMS Collaboration

This Letter presents the observation of the rare Z boson decay Z -> psi l(+)l(-). Here, psi represents contributions from direct J/psi and psi(2S) -> J/psi X, l(+)l(-) is a pair of electrons or muons, and the J/psi meson is detected via its decay to mu(+)mu(-). The sample of proton-proton collision data, collected by the CMS experiment at the LHC at a center--of-mass energy of 13 TeV, corresponds to an integrated luminosity of 35.9 fb(-1). The signal is observed with a significance in excess of 5 standard deviations. After subtraction of the psi(2S) -> J/psi X contribution, the ratio of the branching fraction of the exclusive decay Z -> J/psi X, l(+) l(-) to the decay Z -> mu(+)mu(-)mu(+)mu(-) within a fiducial phase space is measured to be B(Z -> J/psi X, l(+) l(-))/B(Z -> mu(+)mu(-)mu(+)mu(-)) = 0.67 +/- 0.18(stat) +/- 0.05(syst).

PHYSICAL REVIEW LETTERS 121[14], 141801, 2018. DOI: 10.1103/PhysRevLett.121.141801

[P414-2018] "On the mechanical properties of novamene: A fully atomistic molecular dynamics and DFT investigation"

Oliveira, E. F.*; Autreto, P. A. D.*; Woellner, C. F.*; Galvao, D. S.*

We have investigated through fully atomistic reactive molecular dynamics and density functional theory simulations, the mechanical properties and fracture dynamics of single-ringed novamene (1R-novamene), a new 3D carbon allotrope structure recently proposed. Our results showed that 1R-novamene is an anisotropic structure with relation to tensile deformation. Although 1R-novamente shares some mechanical features with other carbon allotropes, it also exhibits distinct ones, such as, extensive structural reconstructions. 1R-novamene presents ultimate strength (similar to 100 GPa) values lower than other carbon allotropes, but it has the highest ultimate strain along the z-direction (similar to 22.5%). Although the Young's modulus (similar to 600 GPa) and ultimate strength values are smaller than for other carbon allotropes, they still outperform other materials, such as for example silicon, steel or titanium alloys. With relation to the fracture dynamics, 1R-novamene is again anisotropic with the fracture/crack propagation originating from deformed heptagons and pentagons for x and y directions and broken sp(3) bonds connecting structural planes. Another interesting feature is the formation of multiple and long carbon linear chains in the final fracture stages.

CARBON 139, 782-788, 2018. DOI: 10.1016/j.carbon.2018.07.038

[P415-2018] "Performance of reconstruction and identification of tau leptons decaying to hadrons and nu(tau) in pp collisions at root s=13 TeV"

Sirunyan, A. M.; Tumasyan, A.; Adam, W.; **Chinellato, J. A.*; Tonelli Manganote, E. J.***; et al.
CMS Collaboration

The algorithm developed by the CMS Collaboration to reconstruct and identify tau leptons produced in proton-proton collisions at root s = 7 and 8 TeV, via their decays to hadrons and a neutrino, has been significantly improved. The changes include a revised reconstruction of pi(0) candidates, and improvements in multivariate discriminants to separate tau leptons from jets and electrons. The algorithm is extended to reconstruct tau leptons in highly Lorentz-boosted pair production, and in the high-level trigger. The performance of the algorithm is studied using proton-proton collisions recorded during 2016 at root s = 13 TeV, corresponding to an integrated luminosity of 35.9 fb(-1). The performance is evaluated in terms of the efficiency for a genuine tau lepton to pass the identification criteria and of the probabilities for jets, electrons, and muons to be misidentified as tau leptons. The results are found to be very close to those expected from Monte Carlo simulation.

JOURNAL OF INSTRUMENTATION 13, P10005, 2018. DOI: 10.1088/1748-0221/13/10/P10005

[P416-2018] "Photothermally modulated magnetic resonance using a light access microwaves cavity: Influence of skin depth and of photo-injected carriers"

Cordeiro, T. C.; Soffner, M. E.; **Mansanares, A. M.***; da Silva, E. C.

This study reports on the modulation frequency dependence of the photothermally modulated magnetic resonance signal of a set of magnetic samples in the form of foils, layers, and thin films: 50 mu m Fe and Ni foils; 5 mu m magnetic layer of gamma-Fe2O3 in a cassette tape; and 150 nm Co and Permalloy films deposited on glass and Si (111) substrates, besides the naked Si substrate. It is shown, both by analytical calculation and by measurements, that the skin depth of the microwaves deeply influences the signal behavior by selecting the portion of the sample that is probed. Clear differences in the frequency dependence are observed between the metallic Ni and Fe foils and the dielectric gamma-Fe2O3 cassette tape. Furthermore, the thermal mismatch between the magnetic films (Co and Permalloy) and substrates (glass and Si) also plays a crucial role, once the modulation of the temperature is strongly dependent on the substrate thermal parameters at low modulation frequencies. The non-resonant signal from the diamagnetic Si is also analyzed. It is produced by the absorption of microwaves by the photo-injected free carriers and presents characteristic behavior in the investigated frequency range. Published by AIP Publishing.

JOURNAL OF APPLIED PHYSICS 124[16], 163901, 2018. DOI: 10.1063/1.5049683

[P417-2018] "Pixelated GaSb solar cells on silicon by membrane bonding"

Mangu, V. S.; Renteria, E. J.; Addamane, S. J.; Mansoori, A.; Armendariz, A.; **Deneke, C. F.***; Ferreira, S. O.; Zamiri, M.; Balakrishnan, G.; Cavallo, F.

We demonstrate thin-film GaSb solar cells which are isolated from a GaSb substrate and transferred to a Si substrate. We epitaxially grow similar to 3.3 mu m thick GaSb P on N diode structures on a GaSb substrate. Upon patterning in 2D arrays of pixels, the GaSb films are released via epitaxial lift-off and they are transferred to Si substrates. Encapsulation of each pixel preserves the structural integrity of the GaSb film during lift-off. Using this technique, we consistently transfer similar to 4 x 4 mm(2) array of pixelated GaSb membranes to a Si substrate with a similar to 80%-100% yield. The area of individual pixels ranges from similar to 90 x 90 mu m(2) to similar to 340 x 340 mu m(2). Further processing to fabricate photovoltaic devices is performed after the transfer. GaSb solar cells with lateral sizes of similar to 340 x 340 mu m(2) under illumination exhibit efficiencies of which compares favorably with extracted values for large-area (i.e., 5 x 5 mm(2)) homoepitaxial GaSb solar cells on GaSb substrates. Published by AIP Publishing.

APPLIED PHYSICS LETTERS 113[12], 123502, 2018. DOI: 10.1063/1.5037800

[P418-2018] "Poole-Frenkel emission on functionalized, multilayered-packed reduced graphene oxide nanoplatelets"

Jimenez, M. J. M.*; de Oliveira, R. F.; Shimizu, F. M.; Bufon, C. C. B.; **Rodrigues, V.***; Gobbi, A. L.; Piazzetta, M. H. O.; **Riul, A.***

The unique electronic, mechanical and optical properties of graphene make it a remarkable 2D material, widely explored in a plethora of applications. However, graphene zero-bandgap and the production of defect-free pristine graphene in large areas still limit some applications. To circumvent these issues, graphene-derived 2D materials have arisen as attractive candidates for low-dimensional systems, which requires a better comprehension of their properties. Here, we report a detailed investigation of the conduction mechanisms of two functionalized reduced graphene oxides (rGOs) nanoplatelets, named GPAH and GPSS. The functionalized rGO nanoplatelets were bottom-up assembled via the layer-by-layer technique, enabling molecular-level thickness control of nanostructures with well-defined composition and structure. For the reported multilayered GPAH/GPSS films the charge carriers followed Mott's law, presenting a typical conduction behavior of 2D systems described by the Poole-Frenkel model. The multilayered GPAH/GPSS nanostructure presented a conductivity of 10(-4)S cm(-1), optical bandgap of similar to 3.3 eV and a relative dielectric permittivity (epsilon(r)) of 6.4. Temperature-dependent I-V measurements indicated a strong variation of er below the critical temperature (T-C = 237 K), associated with a high dipole reorientation in the formed GPAH/GPSS nanostructure. All these characteristics make the GPAH/GPSS nanocomposite attractive for graphene-oriented applications, such as electronic devices.

NANOTECHNOLOGY 29[50], 505703, 2018. DOI: 10.1088/1361-6528/aae18e

[P419-2018] "Precision measurement of the structure of the CMS inner tracking system using nuclear interactions"

Sirunyan, A. M.; Tumasyan, A.; Adam, W.; **Chinellato, J. A.*; Tonelli Manganote, E. J.***; et al.
CMS Collaboration

The structure of the CMS inner tracking system has been studied using nuclear interactions of hadrons striking its material. Data from proton-proton collisions at a center-of-mass energy of 13 TeV recorded in 2015 at the LHC are used to reconstruct millions of secondary vertices from these nuclear interactions. Precise positions of the beam pipe and the inner tracking system elements, such as the pixel detector support tube, and barrel pixel detector inner shield and support rails, are determined using these vertices. These measurements are important for detector simulations, detector upgrades, and to identify any changes in the positions of inactive elements.

JOURNAL OF INSTRUMENTATION 13, P10034, 2018. DOI: 10.1088/1748-0221/13/10/P10034

[P420-2018] "Pseudorapidity and transverse momentum dependence of flow harmonics in pPb and PbPb collisions"

Sirunyan, A. M.; Tumasyan, A.; **Chinellato, J. A.*; Tonelli Manganote, E. J.***; et al.
CMS Collaboration

Measurements of azimuthal angular correlations are presented for high-multiplicity pPb collisions at root s(NN) = 5.02 TeV and peripheral PbPb collisions at root s(NN) = 2.76 TeV. The data used in this work were collected with the Compact Muon Solenoid (CMS) detector at the European Organization for Nuclear Research (CERN) Large Hadron Collider (LHC). Fourier coefficients as functions of transverse momentum and pseudorapidity are studied using the scalar product method; four-, six-, and eight-particle cumulants; and the Lee-Yang zero technique. The influence of event plane decorrelation is evaluated using the scalar product method and found to account for most of the observed pseudorapidity dependence.

PHYSICAL REVIEW C 98[4], 044902, 2018. DOI: 10.1103/PhysRevC.98.044902

[P421-2018] "Rapidly evolving transients in the Dark Energy Survey"

Pursiainen, M.; Childress, M.; Smith, M.; **Sobreira, F.***; et al.
DES Collaboration

We present the results of a search for rapidly evolving transients in the Dark Energy Survey Supernova Programme. These events are characterized by fast light-curve evolution (rise to peak in less than or similar to 10 d and exponential decline in less than or similar to 30 d after peak). We discovered 72 events, including 37 transients with a spectroscopic redshift from host galaxy spectral features. The 37 events increase the total number of rapid optical transients by more than a factor of two. They are found at a wide range of redshifts (0.05 < z < 1.56) and peak brightnesses (-15.75 > M-g > -22.25). The multiband photometry is well fit by a blackbody up to few weeks after peak. The events appear to be hot (T approximate to 10 000-30 000 K) and large (R approximate to 10(14) -2 x 10(15) cm) at peak, and generally expand and cool in time, though some events show evidence for a receding photosphere with roughly constant temperature. Spectra taken around peak are dominated by a blue featureless continuum consistent with hot, optically thick ejecta. We compare our events with a previously suggested physical scenario involving shock breakout in an optically thick wind surrounding a core-collapse supernova, we conclude that current models for such a scenario might need an additional power source to describe the exponential decline. We find that these transients tend to favour star-forming host galaxies, which could be consistent with a core-collapse origin. However, more detailed modelling of the light curves is necessary to determine their physical origin.

MONTHLY NOTICES OF THE ROYAL ASTRONOMICAL SOCIETY 481[1], 894-917, 2018. DOI: 10.1093/mnras/sty2309

[P422-2018] "Role of electronic and structural characteristics on the magnetic properties of the Gd3Co1-xRux series"

Monteiro, J. C. B.*; dos Reis, R.; **Gandra, F. G.***

We report a systematic study to unveil the major magnetic and calorimetric behavior differences between Gd3Co and Gd3Ru compounds. We focus on the investigation of the microscopic origin of the enhanced magnetocaloric properties presented by Gd3Ru through an analysis of the magnetization, structural and calorimetric properties of the Gd3Co1-xRux series. Chemical substitution and hydrostatic pressure were used as tools to determine the differences between the structural and electronic changes within the series. Our experimental data and DFT calculations suggest that while the structural changes causes almost no effect on the magnetic properties of the compounds, the hybridization between the gadolinium 5d and the transition metal 3d(4d) orbitals plays a fundamental role and regulate the magnetic interaction in the series.

JOURNAL OF ALLOYS AND COMPOUNDS 768, 1-5, 2018. DOI: 10.1016/j.jallcom.2018.07.210

[P423-2018] "Search for a heavy resonance decaying into a Z boson and a Z or W boson in 2l2q final states at root s=13 TeV"

Sirunyan, A. M.; Tumasyan, A.; Adam, W.; **Chinellato, J. A.*; Tonelli Manganote, E. J.***; et al.
CMS Collaboration

A search has been performed for heavy resonances decaying to ZZ or ZW in 2l2q final states, with two charged leptons (l = e, mu) produced by the decay of a Z boson, and two quarks produced by the decay of a W or Z boson. The analysis is sensitive to resonances with masses in the range from 400 to 4500 GeV. Two categories are defined based on the merged or resolved reconstruction of the hadronically decaying vector boson, optimized for high- and low-mass resonances, respectively. The search is based on data collected during 2016 by the CMS experiment at the LHC in proton-proton collisions with a center-of-mass energy of root s = 13 TeV, corresponding to an integrated luminosity of 35.9 fb(-1). No excess is observed in the data above the standard model background expectation. Upper limits on the production cross section of heavy, narrow spin-1 and spin-2 resonances are derived as a function of the resonance mass, and exclusion limits on the production of W' bosons and bulk graviton particles are calculated in the framework of the heavy vector triplet model and warped extra dimensions, respectively.

JOURNAL OF HIGH ENERGY PHYSICS 9, 101, 2018. DOI: 10.1007/JHEP09(2018)101

[P424-2018] "Search for an exotic decay of the Higgs boson to a pair of light pseudoscalars in the final state of two muons and two tau leptons in proton-proton collisions at TeV"

Sirunyan, A. M.; Tumasyan, A.; Adam, W.; **Chinellato, J. A.*; Tonelli Manganote, E. J.***; et al.
CMS Collaboration

A search for exotic Higgs boson decays to light pseudoscalars in the final state of two muons and two tau leptons is performed using proton-proton collision data recorded by the CMS experiment at the LHC at a center-of-mass energy of 13 TeV in 2016, corresponding to an integrated luminosity of 35.9 fb(-1). Masses of the pseudoscalar boson between 15.0 and 62.5 GeV are probed, and no significant excess of data is observed above the prediction of the standard model. Upper limits are set on the branching fraction of the Higgs boson to two light pseudoscalar bosons in different types of two-Higgs--doublet models extended with a complex scalar singlet.

JOURNAL OF HIGH ENERGY PHYSICS [11], 018, 2018. DOI: 10.1007/JHEP11(2018)018

[P425-2018] "Search for an exotic decay of the Higgs boson to a pair of light pseudoscalars in the final state with two bquarks and two tau leptons in proton-proton collisions at root s=13 TeV"

Sirunyan, A. M.; Tumasyan, A.; **Chinellato, J. A.*; Tonelli Manganote, E. J.***; et al.
CMS Collaboration

A search for an exotic decay of the Higgs boson to a pair of light pseudoscalar bosons is performed for the first time in the final state with two b quarks and two tau leptons. The search is motivated in the context of models of physics beyond the standard model (SM), such as two Higgs doublet models extended with a complex scalar singlet (2HDM + S), which include the next-to-minimal supersymmetric SM (NMSSM). The results are based on a data set of proton-proton collisions corresponding to an integrated luminosity of 35.9 fb(-1), accumulated by the CMS experiment at the LHC in 2016 at a center-of-mass energy of 13 TeV. Masses of the pseudoscalar boson between 15 and 60 GeVare probed, and no excess of events above the SM expectation is observed. Upper limits between 3 and 12% are set on the branching fraction B(h -> aa -> 2 tau 2b) assuming the SM production of the Higgs boson. Upper limits are also set on the branching fraction of the Higgs boson to two light pseudoscalar bosons in different 2HDM + S scenarios. Assuming the SM production cross section for the Higgs boson, the upper limit on this quantity is as low as 20% for a mass of the pseudoscalar of 40 GeV in the NMSSM.

PHYSICS LETTERS B 785, 462-488, 2018. DOI: 10.1016/j.physletb.2018.08.057

[P426-2018] "Search for black holes and sphalerons in high--multiplicity final states in proton-proton collisions a root s=13 TeVt"

Sirunyan, A. M.; Tumasyan, A.; Adam, W.; **Chinellato, J. A.*; Tonelli Manganote, E. J.***; et al.
CMS Collaboration

A search in energetic, high-multiplicity final states for evidence of physics beyond the standard model, such as black holes, string balls, and electroweak sphalerons, is presented. The data sample corresponds to an integrated luminosity of 35.9 fb(-1) collected with the CMS experiment at the LHC in proton-proton collisions at a center-of-mass energy of 13 TeV in 2016. Standard model backgrounds, dominated by multijet production, are determined from control regions in data without any reliance on simulation. No evidence for excesses above the predicted background is observed. Model-independent 95% confidence level upper limits on the cross section of beyond the standard model signals in these final states are set and further interpreted in terms of limits on semiclassical black hole, string ball, and sphaleron production. In the context of models with large extra dimensions, semiclassical black holes with minimum masses as high as 10.1 TeV and string balls with masses as high as 9.5 TeV are excluded by this search. Results of the first dedicated search for electroweak sphalerons are presented. An upper limit of 0.021 is set at 95% confidence level on the fraction of all quark-quark interactions above the nominal threshold energy of 9 TeV resulting in the sphaleron transition.

JOURNAL OF HIGH ENERGY PHYSICS [11], 042, 2018. DOI: 10.1007/JHEP11(2018)042

[P427-2018] "Search for dark matter produced in association with a Higgs boson decaying to gamma gamma or tau(+) tau(-) at root s=13 TeV"

Sirunyan, A. M.; Tumasyan, A.; Adam, W.; **Chinellato, J. A.*; Tonelli Manganote, E. J.***; et al.
CMS Collaboration

A search for dark matter particles is performed by looking for events with large transverse momentum imbalance and a recoiling Higgs boson decaying to either a pair of photons or a pair of tau leptons. The search is based on proton-proton collision data at a center-of-mass energy of 13 TeV collected at the CERN LHC in 2016 and corresponding to an integrated luminosity of 35.9 fb(-1). No significant excess over the expected standard model background is observed. Upper limits at 95% confidence level are presented for the product of the production cross section and branching fraction in the context of two benchmark simplified models. For the Z'-two-Higgs-doublet model (where Z' is a new massive boson mediator) with an intermediate heavy pseudoscalar particle of mass m(A) = 300 GeV and m(DM) = 100 GeV, the Z' masses from 550 GeV to 1265 GeV are excluded. For a baryonic Z' model, with m(DM) = 1 GeV, Z' masses up to 615 GeV are excluded. Results are also presented for the spin--independent cross section for the dark matter-nucleon interaction as a function of the mass of the dark matter particle. This is the first search for dark matter particles produced in association with a Higgs boson decaying to two tau leptons.

JOURNAL OF HIGH ENERGY PHYSICS 9, 046, 2018. DOI: 10.1007/JHEP09(2018)046

[P428-2018] "Search for long-lived particles with displaced vertices in multijet events in proton-proton collisions at root s=13 TeV"

Sirunyan, A. M.; Tumasyan, A.; Adam, W.; **Chinellato, J. A.*; Tonelli Manganote, E. J.***; et al.
CMS Collaboration

Results are reported from a search for long-lived particles in proton-proton collisions at root s = 13 TeV delivered by the CERN LHC and collected by the CMS experiment. The data sample, which was recorded during 2015 and 2016, corresponds to an integrated luminosity of 38.5 fb(-1). This search uses benchmark signal models in which long-lived particles are pair-produced and each decays into two or more quarks, leading to a signal with multiple jets and two displaced vertices composed of many tracks. No events with two well-separated high-track-multiplicity vertices are observed. Upper limits are placed on models of R-parity violating supersymmetry in which the long-lived particles are neutralinos or gluinos decaying solely into multijet final states or top squarks decaying solely into dijet final states. For neutralino, gluino, or top squark masses between 800 and 2600 GeV and mean proper decay lengths between 1 and 40 mm, the analysis excludes cross sections above 0.3 fb at 95% confidence level. Gluino and top squark masses are excluded below 2200 and 1400 GeV, respectively, for mean proper decay lengths between 0.6 and 80 mm. A method is provided for extending the results to other models with pair-produced long-lived particles.

PHYSICAL REVIEW D 98[9], 092011, 2018. DOI: 10.1103/PhysRevD.98.092011

[P429-2018] "Search for new physics in dijet angular distributions using proton-proton collisions at root s=13 TeV and constraints on dark matter and other models"

Sirunyan, A. M.; Tumasyan, A.; Adam, W.; **Chinellato, J. A.*; Tonelli Manganote, E. J.***; et al.
CMS Collaboration

Search is presented for physics beyond the standard model, based on measurements of dijet angular distributions in proton-proton collisions at root s = 13 TeV. The data collected with the CMS detector at the LHC correspond to an integrated luminosity of 35.9 fb(-1). The observed distributions, corrected to particle level, are found to be in agreement with predictions from perturbative quantum chromodynamics that include electroweak corrections. Constraints are placed on models containing quark contact interactions, extra spatial dimensions, quantum black holes, or dark matter, using the detector-level distributions. In a benchmark model where only left-handed quarks participate, contact interactions are excluded at the 95% confidence level up to a scale of 12.8 or 17.5 TeV, for destructive or constructive interference, respectively.

The most stringent lower limits to date are set on the ultraviolet cutoff in the Arkani-Hamed-Dimopoulos-Dvali model of extra dimensions. In the Giudice-Rattazzi-Wells convention, the cutoff scale is excluded up to 10.1 TeV. The production of quantum black holes is excluded for masses below 5.9 and 8.2 TeV, depending on the model. For the first time, lower limits between 2.0 and 4.6 TeV are set on the mass of a dark matter mediator for (axial-) vector mediators, for the universal quark coupling g(q) = 1.0.

EUROPEAN PHYSICAL JOURNAL C 78[9], 789, 2018. DOI: 10.1140/epjc/s10052-018-6242-x

[P430-2018] "Search for Pair-Produced Resonances Each Decaying into at Least Four Quarks in Proton-Proton Collisions at root s=13 TeV"

Sirunyan, A. M.; Tumasyan, A.; **Chinellato, J. A.*; Tonelli Manganote, E. J.***; et al.
CMS Collaboration

This Letter presents the results of a search for pair-produced particles of masses above 100 GeV that each decay into at least four quarks. Using data collected by the CMS experiment at the LHC in 2015-2016, corresponding to an integrated luminosity of 38.2 fb(-1), reconstructed particles are clustered into two large jets of similar mass, each consistent with four-parton substructure. No statistically significant excess of data over the background prediction is observed in the distribution of average jet mass. Pair-produced squarks with dominant hadronic R-parity--violating decays into four quarks and with masses between 0.10 and 0.72 TeV are excluded at 95% confidence level. Similarly, pair-produced gluinos that decay into five quarks are also excluded with masses between 0.10 and 1.41 TeV at 95% confidence level. These are the first constraints that have been placed on pair-produced particles with masses below 400 GeV that decay into four or five quarks, bridging a significant gap in the coverage of R-parity-violating supersymmetry parameter space.

PHYSICAL REVIEW LETTERS 121[14], 141802, 2018. DOI: 10.1103/PhysRevLett.121.141802

[P431-2018] "Search for physics beyond the standard model in high-mass diphoton events from proton-proton collisions at root s=13 TeV"

Sirunyan, A. M.; Tumasyan, A.; Adam, W.; **Chinellato, J. A.*; Tonelli Manganote, E. J.***; et al.
CMS Collaboration

A search for physics beyond the standard model is performed using a sample of high-mass diphoton events produced in proton-proton collisions at root s = 13 TeV. The data sample was collected in 2016 with the CMS detector at the LHC and corresponds to an integrated luminosity of 35.9 fb(-1). The search is performed for both resonant and nonresonant new physics signatures. At 95% confidence level, lower limits on the mass of the first Kaluza-Klein excitation of the graviton in the Randall-Sundrum warped extradimensional model are determined to be in the range of 2.3 to 4.6 TeV, for values of the associated coupling parameter between 0.01 and 0.2. Lower limits on the production of scalar resonances and modelindependent cross section upper limits are also provided. For the large extra-dimensional model of Arkani-amed, Dimopoulos, and Dvali, lower limits are set on the string mass scale M-S ranging from 5.6 to 9.7 TeV, depending on the model parameters. The first exclusion limits are set in the two-dimensional parameter space of a continuum clockwork model.

PHYSICAL REVIEW D 98[9], 092001, 2018. DOI: 10.1103/PhysRevD.98.092001

[P432-2018] "Search for the decay of a Higgs boson in the ll gamma channel in proton-proton collisions at root s=13 TeV"

Sirunyan, A. M.; Tumasyan, A.; Adam, W.; **Chinellato, J. A.*; Tonelli Manganote, E. J.***; et al
CMS Collaboration

A search for a Higgs boson decaying into a pair of electrons or muons and a photon is described. Higgs boson decays to a Z boson and a photon (H Z , = e or), or to two photons, one of which has an internal conversion into a muon pair (H (*)) were considered. The analysis is performed using a data set recorded by the CMS experiment at the LHC from proton--proton collisions at a center-of-mass energy of 13 TeV, corresponding to an integrated luminosity of 35.9 fb(-1). No significant excess above the background prediction has been found. Limits are set on the cross section for a standard model Higgs boson decaying to opposite-sign electron or muon pairs and a photon. The observed limits on cross section times the corresponding branching fractions vary between 1.4 and 4.0 (6.1 and 11.4) times the standard model cross section for H (*) (H Z) in the 120-130 GeV mass range of the system. The H (*) and H Z analyses are combined for m(H) =125GeV, obtaining an observed (expected) 95% confidence level upper limit of 3.9 (2.0) times the standard model cross section.

JOURNAL OF HIGH ENERGY PHYSICS [11], 152, 2018. DOI: 10.1007/JHEP11(2018)152

[P433-2018] "Search for top squarks and dark matter particles in opposite-charge dilepton final states at root s=13 TeV"

Sirunyan, A. M.; Tumasyan, A.; Adam, W.; **Chinellato, J. A.*; Tonelli Manganote, E. J.***; et al.
CMS Collaboration

A search for new physics is presented in final states with two oppositely charged leptons (electrons or muons), jets identified as originating from b quarks, and missing transverse momentum (p(T)(miss)). The search uses proton-proton collision data at root s = 13 TeV amounting to 35.9 fb(-1) of integrated luminosity collected using the CMS detector in 2016. Hypothetical signal events are efficiently separated from the dominant t (t) over bar background with requirements on p(T)(miss) and transverse-mass variables. No significant deviation is observed from the expected background. Exclusion limits are set in the context of simplified supersymmetric models with pair-produced top squarks. For top squarks, decaying exclusively to a top quark and a neutralino, exclusion limits are placed at 95% confidence level on the mass of the lightest top squark up to 800 GeVand on the lightest neutralino up to 360 GeV. These results, combined with searches in the single-lepton and all--jet final states, raise the exclusion limits up to 1050 GeV for the lightest top squark and up to 500 GeV for the lightest neutralino. For top squarks undergoing a cascade decay through charginos and sleptons, the mass limits reach up to 1300 GeV for top squarks and up to 800 GeV for the lightest neutralino. The results are also interpreted in a simplified model with a dark matter (DM) particle coupled to the top quark through a scalar or pseudoscalar mediator. For light DM, mediator masses up to 100 (50) GeV are excluded for scalar (pseudoscalar) mediators. The result for the scalar mediator achieves some of the most stringent limits to date in this model.

PHYSICAL REVIEW D 97[3], 032009, 2018. DOI: 10.1103/PhysRevD.97.032009

[P434-2018] "Search for top squarks decaying via four-body or chargino-mediated modes in single-lepton final states in proton-proton collisions at root s=13 TeV"

Sirunyan, A. M.; Tumasyan, A.; Adam, W.; **Chinellato, J. A.*; Manganote, E. J. Tonelli***; et al.
CMS Collaboration

A search for the pair production of the lightest supersymmetric partner of the top quark ((t) over tilde (1)) is presented. The search focuses on a compressed scenario where the mass difference between the top squark and the lightest supersymmetric particle, often considered to be the lightest neutralino ((chi) over tilde (0)(1)), is smaller than the mass of the W boson. The proton-proton collision data were recorded by the CMS experiment at a centre-of-mass energy of 13 TeV, and correspond to an integrated luminosity of 35.9 fb(-1). In this search, two decay modes of the top squark are considered: a four-body decay into a bottom quark, two additional fermions, and a (chi) over tilde (1)(0); and a decay via an intermediate chargino. Events are selected using the presence of a high--momentum jet, significant missing transverse momentum, and a low transverse momentum electron or muon. Two analysis techniques are used, targeting different decay modes ((t) over tilde (1)): of the a sequential selection and a multivariate technique. No evidence for the production of top squarks is found, and mass limits at 95% confidence level are set that reach up to 560 GeV, depending on the m((t) over tilde (1)) - m((chi) over tilde (0)(1)) mass difference and the decay mode.

JOURNAL OF HIGH ENERGY PHYSICS 9, 065, 2018. DOI: 10.1007/JHEP09(2018)065

[P435-2018] "Search for Z gamma resonances using leptonic and hadronic final states in proton-proton collisions at root s=13 TeV"

Sirunyan, A. M.; Tumasyan, A.; Adam, W.; **Chinellato, J. A.*; Tonelli Manganote, E. J.***; et al.
CMS Collaboration

A search is presented for resonances decaying to a Z boson and a photon. The analysis is based on data from proton-proton collisions at a center-of-mass energy of 13 TeV, corresponding to an integrated luminosity of 35.9 fb(-1), and collected with the CMS detector at the LHC in 2016. Two decay modes of the Z boson are investigated. In the leptonic channels, the Z boson candidates are reconstructed using electron or muon pairs. In the hadronic channels, they are identified using a large-radius jet, containing either light-quark or b quark decay products of the Z boson, via jet substructure and advanced b quark tagging techniques. The results from these channels are combined and interpreted in terms of upper limits on the product of the production cross section and the branching fraction to Z gamma for narrow and broad spin-0 resonances with masses between 0.35 and 4.0 TeV, providing thereby the most stringent limits on such resonances.

JOURNAL OF HIGH ENERGY PHYSICS 9, 148, 2018. DOI: 10.1007/JHEP09(2018)148

[P436-2018] "Selective contrast agents with potential to the earlier detection of tumors: Insights on synthetic pathways, physicochemical properties and performance in MRI assays"

Schneider, M. G. M.; Martin, M. J.; Coral, D. F.; **Muraca, D.***; Gentili, C.; van Raap, M. F.; Lassalle, V. L.

Magnetic iron oxide nanoparticles (MNPs) have been prepared and stabilized with three organic acids (tartaric, malic and ascorbic) in order to obtain biocompatible and water dispersible MNPs with potential to bind specifically to tumoral cancer cells. An in deep characterization was performed aiming to verify the presence and effect of the coating and stabilizer on MNPs surface. Besides the mechanisms followed by the different acids to bind MNPs were elucidated and used to justify the differences in the physicochemical properties of each formulation. Data related to characterization revealed that MNPs coated with ascorbic acid (MNPs-AA) resulted the most suitable in terms of their size, surface charge and stability along the time. Besides, ascorbic acid may be recognized by GLUTs receptors that are overexpressed in several kinds of tumoral cells. Therefore, MNPs-AA was selected to explore its performance in both MRI and in vitro assays using human colon cancer cells HCT 116. MRI experiments were performed in clinical equipment using a series of aqueous dispersions of MNPs-AA that were evaluated as T-2 contrast agent. The T-2- weighted images obtained as well as the calculated( )r2,( )indicated that MNPs-AA could act as efficient T-2 contrast agent for MRI. Regarding in vitro assays, MNPs-AA did not alter the cellular function neither exert cytotoxicity using the three explored doses. The internalization of the nanoparticles on the cellular structure was confirmed quanti and qualitatively using atomic absorption spectroscopy and Prussian blue techniques respectively. From these results, it emerges that ascorbic acid coated-magnetite nanoparticles may be used as alternative contrast agent to avoid or minimize some toxicological issues related to the widely used gadolinium.

COLLOIDS AND SURFACES B-BIOINTERFACES 170, 470-478, 2018. DOI: 10.1016/j.colsurfb.2018.06.044

[P437-2018] "Step-by-step synthesis of iron-oxide nanoparticles attached to graphene oxide: A study on the composite properties and architecture"

Tancredi, P.; **Londono, O. M.***; Rojas, P. C. R.; **Knobel, M.***; Socolovsky, L. M.

A set of nanocomposites made of iron oxide nanoparticles covalently bonded to graphene oxide and reduced graphene oxide was successfully prepared. The synthesis was carried out in a precise step-by-step process in order to carefully control the nanocomposite formation. The nanocomposites were characterized by a range of techniques to verify the components arrangement according to the proposed strategy. Over the different samples, an in-depth study by Small Angle X-Ray Scattering (SAXS) and DC-Magnetometry was accomplished to analyze in detail the structure and properties of the systems. The results from this work indicate that the increase of the nanoparticle to graphene oxide ratio and the chemical reduction from graphene oxide to reduced graphene oxide modify the spatial distribution and the architecture of the nanoparticles over the sheets, leading to the formation of localized assemblies and bundle-like structures that have a significant impact on the macroscopicmagnetic behavior.

MATERIALS RESEARCH BULLETIN 107, 255-263, 2018. DOI: 10.1016/j.materresbull.2018.08.003

[P438-2018] "Strain Sensitivity Enhancement of a Sensing Head Based on ZEONEX Polymer FBG in Series With Silica Fiber"

Oliveira, R. ; Bilro, L.; **Marques, T. H. R.*; Cordeiro, C. M. B.***; Nogueira, R.

This study presents the use of a sensing device composed of an all ZEONEX-480R polymer fiber Bragg grating, in series with a silica fiber, for the control/enhancement of the strain sensitivity. The results show that the amount of strain imposed in the total gauge length is unequally distributed in each fiber section. The low Young's modulus and diameter of the polymer fiber employed, compared to the silica one, leads to a higher strain density in the former. Additionally, the control of the length of each fiber section plays also an important role on the distribution of strain in each fiber. Theoretical results show that higher strain sensitivities are easier to achieve for short and long polymer and silica fiber lengths, respectively.

Experimental characterization of a sensing head composed by a 2.6 cm polymer optical fiber and different lengths of silica fiber, led us to control and improve the strain sensitivity of the sensing device.

JOURNAL OF LIGHTWAVE TECHNOLOGY 36[22], 5106-5112, 2018. DOI: 10.1109/JLT.2018.2870054

[P439-2018] "Study of jet quenching with isolated-photon plus jet correlations in PbPb and pp collisions at root s(NN)=5.02 TeV"

Sirunyan, A. M.; Tumasyan, A.; **Chinellato, J. A.*; Tonelli Manganote, E. J.***; et al.
CMS Collaboration

Measurements of azimuthal angle and transverse momentum (p(T)) correlations of isolated photons and associated jets are reported for pp and PbPb collisions at root s(NN) = 5.02 TeV. The data were recorded with the CMS detector at the CERN LHC. For events containing a leading isolated photon with p(T) (gamma) > 40 GeV/c and an associated jet with p(T)(jet) > 30 GeV/c, the photon+jet azimuthal correlation and p(T) imbalance in PbPb collisions are studied as functions of collision centrality and p(T)(gamma). The results are compared to pp reference data collected at the same collision energy and to predictions from several theoretical models for parton energy loss. No evidence of broadening of the photon+jet azimuthal correlations is observed, while the ratio p(T)(jet)/p(T)(gamma) decreases significantly for PbPb data relative to the pp reference. All models considered agree within uncertainties with the data. The number of associated jets per photon with p(T) (gamma) > 80GeV/c is observed to be shifted towards lower p(T)(jet) in central PbPb collisions compared to pp collisions.

PHYSICS LETTERS B 785, 14-39, 2018. DOI: 10.1016/j.physletb.2018.07.061

[P440-2018] "The Dark Energy Survey: Data Release 1"

Abbott, T. M. C.; Abdalla, F. B.; Allam, S.; **Sobreira, F.***; et al.
DES Collaboration; NOAO Data Lab

We describe the first public data release of the Dark Energy Survey, DES DR1, consisting of reduced single-epoch images, co-added images, co-added source catalogs, and associated products and services assembled over the first 3 yr of DES science operations. DES DR1 is based on optical/near-infrared imaging from 345 distinct nights (2013 August to 2016 February) by the Dark Energy Camera mounted on the 4 m Blanco telescope at the Cerro Tololo InterAmerican Observatory in Chile. We release data from the DES wide-area survey covering similar to 5000 deg(2) of the southern Galactic cap in five broad photometric bands, grizY. DES DR1 has a median delivered point-spread function of g = 1.12, r = 0.96, i = 0.88, z = 0.84, and Y = 0.'' 90 FWHM, a photometric precision of <1% in all bands, and an astrometric precision of 151 mas. The median co-added catalog depth for a 1.'' 95 diameter aperture at signal-to-noise ratio (S/N) = 10 is g = 24.33, r = 24.08, i = 23.44, z = 22.69, and Y = 21.44 mag. DES DR1 includes nearly 400 million distinct astronomical objects detected in similar to 10,000 co-add tiles of size 0.534 deg(2) produced from similar to 39,000 individual exposures. Benchmark galaxy and stellar samples contain similar to 310 million and similar to 80 million objects, respectively, following a basic object quality selection. These data are accessible through a range of interfaces, including query web clients, image cutout servers, jupyter notebooks, and an interactive co-add image visualization tool. DES DR1 constitutes the largest photometric data set to date at the achieved depth and photometric precision.

ASTROPHYSICAL JOURNAL SUPPLEMENT SERIES 239[2], 18, 2018. DOI: 10.3847/1538-4365/aae9f0

[P441-2018] "The First Tidally Disrupted Ultra-faint Dwarf Galaxy?: A Spectroscopic Analysis of the Tucana III Stream"

Li, T. S.; Simon, J. D.; **Sobreira, F.***; et al.
DES Collaboration

We present a spectroscopic study of the tidal tails and core of the Milky Way satellite Tucana III, collectively referred to as the Tucana III stream, using the 2dF+AAOmega spectrograph on the Anglo-Australian Telescope and the IMACS spectrograph on the Magellan Baade Telescope. In addition to recovering the brightest nine previously known member stars in the Tucana III core, we identify 22 members in the tidal tails. We observe strong evidence for a velocity gradient of 8.0 +/- 0.4 km s(-1) deg(-1) over at least 3 degrees on the sky. Based on the continuity in velocity, we confirm that the Tucana III tails are real tidal extensions of Tucana III. The large velocity gradient of the stream implies that Tucana III is likely on a radial orbit. We successfully obtain metallicities for four members in the core and 12 members in the tails. We find that members close to the ends of the stream tend to be more metal-poor than members in the core, indicating a possible metallicity gradient between the center of the progenitor halo and its edge. The spread in metallicity suggests that the progenitor of the Tucana III stream is likely a dwarf galaxy rather than a star cluster. Furthermore, we find that with the precise photometry of the Dark Energy Survey data, there is a discernible color offset between metal-rich disk stars and metal-poor stream members. This metallicity-dependent color offers a more efficient method to recognize metal-poor targets and will increase the selection efficiency of stream members for future spectroscopic follow-up programs on stellar streams.

ASTROPHYSICAL JOURNAL 866[1], 22, 2018. DOI: 10.3847/1538-4357/aadf91

[P442-2018] "The Machado-Joseph disease-associated expanded form of ataxin-3: Overexpression, purification, and preliminary biophysical and structural characterization"

Contessotto, M. G. G.; Rosselli-Murai, L. K.; Garcia, M. C. C.; Oliveira, C. L. P.; **Torriani, I. L.***; **Lopes-Cendes, I.***; Murai, M. J.

An expansion of the polyglutamine (polyQ) tract within the deubiquitinase ataxin-3 protein is believed to play a role in a neurodegenerative disorder. Ataxin-3 contains a Josephin catalytic domain and a polyQ tract that renders it intrinsically prone to aggregate, and thus full-length protein is difficult to characterize structurally by high-resolution methods. We established a robust protocol for expression and purification of wild-type and expanded ataxin-3, presenting 19Q and 74Q, respectively. Both proteins are monodisperse as assessed by analytical size exclusion chromatography. Initial biophysical characterization was performed, with apparent transition melting temperature of expanded ataxin-3 lower than the wild--type counterpart. We further characterize the molecular envelope of wild-type and expanded polyQ tract in ataxin-3 using small angle X-ray scattering (SAXS). Characterization of protein-protein interactions between ataxin-3 and newly identified binding partners will benefit from our protocol.

PROTEIN EXPRESSION AND PURIFICATION 152, 40-45, 2018. DOI: 10.1016/j.pep.2018.07.005

[P443-2018] "The STRong lensing Insights into the Dark Energy Survey (STRIDES) 2016 follow-up campaign - I. Overview and classification of candidates selected by two techniques"

Treu, T.; Agnello, A.; Baumer, M. A.; **Sobreira, F.***; et al.

The primary goals of the STRong lensing Insights into the Dark Energy Survey (STRIDES) collaboration are to measure the dark energy equation of state parameter and the free streaming length of dark matter. To this aim, STRIDES is discovering strongly lensed quasars in the imaging data of the Dark Energy Survey and following them up to measure time delays, high resolution imaging, and spectroscopy sufficient to construct accurate lens models. In this paper, we first present forecasts for STRIDES. Then, we describe the STRIDES classification scheme, and give an overview of the Fall 2016 follow-up campaign. We continue by detailing the results of two selection methods, the outlier selection technique and a morphological algorithm, and presenting lens models of a system that could possibly be a lensed quasar in an unusual configuration. We conclude with the summary statistics of the Fall 2016 campaign. Including searches presented in companion papers (Anguita et al.; Ostrovski et al.), STRIDES followed up 117 targets identifying 7 new strongly lensed systems, and 7 nearly identical quasars, which could be confirmed as lenses by the detection of the lens galaxy. 76 candidates were rejected and 27 remain otherwise inconclusive, for a success rate in the range of 6-35 per cent. This rate is comparable to that of previous searches like SDSS Quasar Lens Search even though the parent data set of STRIDES is purely photometric and our selection of candidates cannot rely on spectroscopic information.

MONTHLY NOTICES OF THE ROYAL ASTRONOMICAL SOCIETY, 481, 1, 1041-1054, 2018. DOI: 10.1093/mnras/sty2329

[P444-2018] "The STRong lensing Insights into the Dark Energy Survey (STRIDES) 2016 follow-up campaign - II. New quasar lenses from double component fitting"

Anguita, T.; Schechter, P. L.; Kuropatkin, N.; **Sobreira, F.***; et al.

We report upon the follow-up of 34 candidate lensed quasars found in the Dark Energy Survey using NTTEFOSC, Magellan--IMACS, KECK-ESI, and SOAR-SAMI. These candidates were selected by a combination of double component fitting, morphological assessment, and colour analysis. Most systems followed up are indeed composed of at least one quasar image and 13 with two or more quasar images: two lenses, four projected binaries, and seven nearly identical quasar pairs (NIQs). The two systems confirmed as genuine gravitationally lensed quasars are one quadruple at z(s) = 1.713 and one double at z(s) = 1.515. Lens modelling of these two systems reveals that both systems require very little contribution from the environment to reproduce the image configuration. Nevertheless, small flux anomalies can be observed in one of the images of the quad. Further observations of nine inconclusive systems (including seven NIQs) will allow to confirm (or not) their gravitational lens nature.

MONTHLY NOTICES OF THE ROYAL ASTRONOMICAL SOCIETY 480[4], 5017-5028, 2018. DOI: 10.1093/mnras/sty2172

[P445-2018] "Theoretical Insights into 1D Transition-Metal Nanoalloys Grown on the NiAl(110) Surface"

Zornio, B. F.; **da Silva, E. Z.***; San-Miguel, M. A.

Metallic nanoalloys are essential because of the synergistic effects rather than the merely additive effects of the metal components. Nanoscience is currently able to produce one--atom-thick linear atomic chains (LACs), and the NiAl(110) surface is a well-rested template used to build them We report file first study based on ab initio density functional theory methods of one-dimensional transition metal (TM) nanoalloys (i.e., LACs) grown on the NiAl(110) surface. This is a comprehensive and detailed computational study of the effect of alloying groups 10 and 11 metals (Pd, Pt, Cu, Ag, and Au) in LACs supported on the NiAl(110) surfaces to elucidate the structural, energetic, and electronic properties. From the TM series studied here, Pt appears to be an energy-stabilization species; meanwhile, Ag has a contrasting behavior. The work function changes because the alloying in LACs was satisfactorily explained from the explicit surface dipole moment calculations using an ab initio calculation-based approach, which captured the electron density redistribution upon building the LAC.

ACS OMEGA 3[8], 8819-8828, 2018. DOI: 10.1021/acsomega.8b00817

[P446-2018] "Thermal Evaporated Bismuth Triiodide (BiI3) Thin Films for Photovoltaic Applications"

Coutinho, N. F.*; Menlo, R. B.*; Borrero, N. F. V.*; Marques, F. C.*

Bismuth triiodide (BiI3) is a potential candidate for application in solar cell due to its good optoelectronic properties and because it is free of toxic elements. It can be used as the absorber material in solar cells or converted into the perovskite-like material MA(3)Bi(2)I(9), suitable also for photovoltaic applications. Bismuth triiodide has been prepared by physical vapour transport (PVT) and by solution process through spin coating. In this work we present optical and structural/topological properties of BiI3 deposited by thermal evaporation under high vacuum. The films are slightly tensile, polycrystalline, homogenously distributed and with good adherence on several substrates, with an indirect bandgap of 1.81 eV, index of refraction of 3.3 (630 nm), photoluminescence centered at 1.74 eV and a Raman peak at 118cm(-1) associated with the A(g) mode.

MRS ADVANCES 3[55], 3233-3236, 2018. DOI: 10.1557/adv.2018.405

[P447-2018] "Total electron scattering cross sections from para-benzoquinone in the energy range 1-200 eV"

Lozano, A., I; Oller, J. C.; Jones, D. B.; **da Costa, R. F.***; Varella, M. T. do N.; Bettega, M. H. F.; da Silva, F. F.; Limao-Vieira, P.; **Lima, M. A. P.***; White, R. D.; Brunger, M. J.; Blanco, F.; Munoz, A.; Garcia, G.

Total electron scattering cross sections, from para-benzoquinone, for impact energies ranging between 1 to 200 eV, have been obtained by measuring the attenuation of a linear electron beam under magnetic confinement conditions. Random uncertainty limits on these values have been found to be within 5%. Systematic errors, due to the axial magnetic beam conditions in combination with the acceptance angle of the detector, have been evaluated by integrating our calculated independent atom model with the screening corrected additivity rule and interference term elastic differential cross sections over that detection acceptance angle. Our previous calculations and measurements on this molecule (Jones et al., J. Chem. Phys., 2018, 148, 124312 and J. Chem. Phys., 2018, 148, 204305), have been compiled and complemented with new elastic and inelastic scattering cross section calculations in order to obtain a comprehensive cross section data base, within the considered energy range, for modelling purposes. The self-consistency of the present data set has been evaluated by simulating the electron transport of 15 eV electrons in para-benzoquinone, and comparing those results with the observed transmitted intensity distribution.

PHYSICAL CHEMISTRY CHEMICAL PHYSICS 20, 34, 22368-22378, 2018. DOI: 10.1039/c8cp03297a

[P448-2018] "Towards superlubricity in nanostructured surfaces: the role of van der Waals forces"

Echeverrigaray, F. G.; de Mello, S. R. S.; Leidens, L. M.; da Costa, M. E. H. M.; **Alvarez, F.*;** Burgo, T. A. L.; Michels, A. F.; Figueroa, C. A.

Hydrogenated amorphous carbon (a-C:H) thin films have a unique combination of properties that are fundamental in mechanical and electromechanical devices aimed at energy efficiency issues. The literature brings a wealth of information about the ultra-low friction (superlubricity) mechanism in a-C:H thin films. However, there is persistent controversy concerning the physicochemical mechanisms of contact mechanics at the atomic/molecular level and the role of electrical interactions at the sliding interface is still a matter of debate. We find that the hydrogenation of the outermost nanostructured surface atomic layers of a-C:H thin films is proportional to the surface potential and also to the friction forces arising at the sliding interface. A higher hydrogen-to-carbon ratio reduces the surface potential, directly affecting frictional forces by a less effective long-term interaction. The structural ultra-low friction (superlubricity) is attributed to a lower polarizability at the outermost nanostructured layer of a-C:H thin films due to a higher hydrogen density, which renders weaker van der Waals forces, in particular London dispersion forces. More hydrogenated nanodomains at the surface of a--C:H thin films are proposed to be used to tailor superlubricity.

PHYSICAL CHEMISTRY CHEMICAL PHYSICS 20[34], 21949-21959, 2018. DOI: 10.1039/c8cp02508h

[P449-2018] "Translational vibration modes-The spectral signature of excess proton transport in water"

Teschke, O.*; Castro, J. R.*; Soares, D. M.*

The water molecular arrangement associated with proton transport was investigated using a water bridge structure in electric field (E) over bar intensities of approximately 10(6) V/m. Excess protons in a moderate electric field induce a water molecular transport in a formed pathway at the water/air interface. This interfacial structural arrangement was characterized by its Raman spectrum assigned for modes in the translational lattice vibration region. By comparing the intensities of translational mode intensity for interfacial water (vertical bar(E) over bar vertical bar = 0) and in water bridges with excess proton transport (vertical bar(E) over bar vertical bar not equal 0), the water molecular configuration change is determined. Interfacial water structural induced changes were also measured by contact angle variation. Published by AIP Publishing.

PHYSICS OF FLUIDS 30[11], 112104, 2018. DOI: 10.1063/1.5053483

[P450-2018] "Transverse momentum spectra and nuclear modification factors of charged particles in pp, p-Pb and Pb--Pb collisions at the LHC"

Acharya, S.; Acosta, F. T.; Adamova, D.; **Albuquerque, D. S. D.*; Chinellato, D. D.*; De Souza, R. D.*; Takahashi, J.***; et al. ALICE Collaboration

We report the measured transverse momentum (pT) spectra of primary charged particles from pp, p-Pb and Pb-Pb collisions at a center-of-mass energy p sNN = 5 : 02TeV in the kinematic range of 0 : 15 < pT < 50 GeV/c and jj < 0 : 8. A signi fi cant improvement of systematic uncertainties motivated the reanalysis of data in pp and Pb-Pb collisions at p sNN = 2 : 76TeV, as well as in p-Pb collisions at p sNN = 5 : 02TeV, which is also presented. Spectra from Pb-Pb collisions are presented in nine centrality intervals and are compared to a reference spectrum from pp collisions scaled by the number of binary nucleon-nucleon collisions. For central collisions, the pT spectra are suppressed by more than a factor of 7 around 6-7 GeV/c with a signi fi cant reduction in suppression towards higher momenta up to 30 GeV/c. The nuclear modi fi cation factor RpPb, constructed from the pp and p-Pb spectra measured at the same collision energy, is consistent with unity above 8 GeV/c. While the spectra in both pp and Pb-Pb collisions are substantially harder at p sNN = 5 : 02TeV compared to 2.76TeV, the nuclear modi fi cation factors show no signi fi cant collision energy dependence. The obtained results should provide further constraints on the parton energy loss calculations to determine the transport properties of the hot and dense QCD matter.

JOURNAL OF HIGH ENERGY PHYSICS [11], 013, 2018. DOI: 10.1007/JHEP11(2018)013

[P451-2018] "Unconventional Multiband Superconductivity in Bulk SrTiO3 and LaAlO3/SrTiO3 Interfaces"

Trevisan, T. V.*; Schutt, M.; Fernandes, R. M.

Although discovered many decades ago, superconductivity in doped SrTiO3 remains a topic of intense research. Recent experiments revealed that, upon increasing the carrier concentration, multiple bands cross the Fermi level, signaling the onset of Lifshitz transitions. Interestingly, T-c was observed to be suppressed across the Lifshitz transition of oxygen-deficient SrTiO3; a similar behavior was also observed in gated LaAlO3/SrTiO3 interfaces. Such a behavior is difficult to explain in the clean theory of two-band superconductivity, as the additional electronic states provided by the second band should enhance T-c. Here, we show that this unexpected behavior can be explained by the strong pair-breaking effect promoted by disorder, which takes place if the interband pairing interaction is subleading and repulsive. A consequence of this scenario is that, upon moving away from the Lifshitz transition, the two-band superconducting state changes from opposite-sign gaps to same-sign gaps.

PHYSICAL REVIEW LETTERS 121[12], 127002, 2018. DOI: 10.1103/PhysRevLett.121.127002

[P452-2018] "Uniaxial-deformation behavior of ice I-h as described by the TIP4P/Ice and mW water models"

Santos-Florez*, P. A.; Ruestes, C. J.; **de Koning, M.***

Using molecular dynamics simulations, we assess the uniaxial deformation response of ice I-h as described by two popular water models, namely, the all-atom TIP4P/Ice potential and the coarse-grained mW model. In particular, we investigate the response to both tensile and compressive uniaxial deformations along the [0001] and [0 (1) over bar 10] crystallographic directions for a series of different temperatures. We classify the respective failure mechanisms and assess their sensitivity to strain rate and cell size. While the TIP4P/Ice model fails by either brittle cleavage under tension at low temperatures or large-scale amorphization/melting, the mW potential behaves in a much more ductile manner, displaying numerous cases in which stress relief involves the nucleation and subsequent activity of lattice dislocations. Indeed, the fact that mW behaves in such a malleable manner even at strain rates that are substantially higher than those applied in typical experiments indicates that the mW description of ice I-h is excessively ductile. One possible contribution to this enhanced malleability is the absence of explicit protons in the mW model, disregarding the fundamental asymmetry of the hydrogen bond that plays an important role in the nucleation and motion of lattice dislocations in ice I-h. Published by AIP Publishing.

JOURNAL OF CHEMICAL PHYSICS 149[16], 164711, 2018. DOI: 10.1063/1.5048517

[P453-2018] "Unraveling the Atomic Structure of Fe Intercalated under Graphene on Ir(111): A Multitechnique Approach"

Ferreira, R. C. D.*; de Lima, L. H.; Barreto, L.; **Silva, C. C.*; Landers, R.*; de Siervo, A.***

The interaction of Fe deposited on graphene grown on Ir(111) was studied in detail to better understand the growth, intercalation, and oxidation of Fe ultrathin films on and under graphene. The study has combined a multiple technique approach that allows extracting at once the chemical, topographic, and precise atomic structure of the system submitted to different conditions of growth and atmospheric environment. For instance, scanning tunneling microscopy (STM) measurements allowed us to follow the formation of Fe nanostructures during Fe deposition and intercalation. Synchrotron-based high-resolution X-ray photoelectron spectroscopy (HR-XPS) untangled the different chemical environments for C-Fe bonds. We have also used photoelectron diffraction experiments to site-specifically unravel the atomic structure of the intercalated Fe under graphene. Oxidation experiments were also performed for samples prepared under different conditions which revealed that indeed one can set the sample temperature to selectively protect or oxidize the intercalated/supported materials, which open interesting possibilities to engineer complex metal-oxide graphene-based devices.

CHEMISTRY OF MATERIALS 30[20], 7201-7210, 2018. DOI: 10.1021/acs.chemmater.8b03186

[P454-2018] "Unraveling the Origin of Operational Instability of Quantum Dot Based Light-Emitting Diodes"

Chang, J. H.; Park, P.; Jung, H.; Jeong, B. G.; Hahm, D.; **Nagamine, G.***; Ko, J.; Cho, J.; **Padilha, L. A.***; Lee, D. C.; Lee, C.; Char, K.; Bae, W. K.

We investigate the operational instability of quantum dot (QD)-based light-emitting diodes (QLEDs). Spectroscopic analysis on the QD emissive layer within devices in chorus with the optoelectronic and electrical characteristics of devices discloses that the device efficiency of QLEDs under operation is indeed deteriorated by two main mechanisms. The first is the luminance efficiency drop of the QD emissive layer in the running devices owing to the accumulation of excess electrons in the QDs, which escalates the possibility of nonradiative Auger recombination processes in the QDs. The other is the electron leakage toward hole transport layers (HTLs) that accompanies irreversible physical damage to the HTL by creating nonradiative recombination centers. These processes are distinguishable in terms of the time scale and the reversibility, but both stem from a single origin, the discrepancy between electron versus hole injection rates into QDs. Based on experimental and calculation results, we propose mechanistic models for the operation of QLEDs in individual quantum dot levels and their degradation during operation and offer rational guidelines that promise the realization of high-performance QLEDs with proven operational stability.

ACS NANO 12[10], 10231-10239, 2018. DOI: 10.1021/acsnano.8b03386

[P455-2018] "Vacuum fluctuations and boundary conditions in a global monopole"

Barroso, V. S.*; Pitelli, J. P. M.

We study the vacuum fluctuations of a massless scalar field (psi) over cap on the background of a global monopole. Due to the nontrivial topology of the global monopole spacetime characterized by a solid deficit angle, parametrized by eta(2), we expect that <(psi) over cap (2)>(ren) and <(T) over cap (mu nu)>(ren) are nonzero and proportional to eta(2), so that they annul in the Minkowski limit eta -> 0. However, due to the naked singularity at the monopole core, the evolution of the scalar field is not unique. In fact, they are in one-to-one correspondence with the boundary conditions which turn into self-adjoint the spatial part of the wave operator. We show that only the Dirichlet boundary condition corresponds to our expectations and gives zero contribution to the vacuum fluctuations in the Minkowski limit. All other boundary conditions give nonzero contributions in this limit due to the nontrivial interaction between the field and the singularity.

PHYSICAL REVIEW D 98, 6, 065009, 2018. DOI: 10.1103/PhysRevD.98.065009

[P456-2018] "Yields and production rates of cosmogenic Li-9 and He-8 measured with the Double Chooz near and far detectors"

de Kerret, H.; Abrahao, T.; Almazan, H.; **Gonzalez, L. F. G.*; Kemp, E.***
Double Chooz Collaboration

The yields and production rates of the radioisotopes Li-9 and He-8 created by cosmic muon spallation on C-12, have been measured by the two detectors of the Double Chooz experiment. The identical detectors are located at separate sites and depths, which means that they are subject to different muon spectra. The near (far) detector has an overburden of approximate to 120 m.w.e. (approximate to 300 m.w.e.) corresponding to a mean muon energy of 32.1 +/- 2.0 GeV (63.7 +/- 5.5 GeV). Comparing the data to a detailed simulation of the Li-9 and He-8 decays, the contribution of the He-8 radioisotope at both detectors is found to be compatible with zero. The observed Li-9 yields in the near and far detectors are 5.51 +/- 0.51 and 7.90 +/- 0.51, respectively, in units of 10(-8-1)g(-1)cm(2). The shallow overburdens of the near and far detectors give a unique insight when combined with measurements by KamLAND and Borexino to give the first multi-experiment, data driven relationship between the Li-9 yield and the mean muon energy according to the power law and Y-0 = (0.43 +/- 0.11) x 10(-8-1)g(-1)cm(2). This relationship gives future liquid scintillator based experiments the ability to predict their cosmogenic Li-9 background rates.

JOURNAL OF HIGH ENERGY PHYSICS 11, 053, 2018. DOI: 10.1007/JHEP11(2018)053

Eventos publicados

[P457-2018] "Core-shell (TiO2@Silica) nanoparticles for random lasers"

Jimenez-Villar, E.*; Mestre, V.; Wetter, N. U.; de Sa, G. F.

Scattering media are of great current interest, due to their potential applications in photovoltaic cells, efficient photocatalyzers, random lasers and novel optical functional devices. Here, we have introduced a core-shell scattering medium for random lasing composed by core-shell nanoparticles (TiO2@Silica) suspended in an ethanol solution of Rhodamine 6G. Higher efficiency, lower laser threshold and long photobleaching lifetime were demonstrated in random laser. A promising method called fraction of absorbed pumping (FAP) has been introduced, which opens a new avenue to characterize and study scattering media. In this article, we also investigate the random laser action at the critical regime of localization by increasing considerably the concentration of TiO2@Silica nanoparticles. Narrow peaks arising in the random laser emission spectrum are observed.

The classical superfluorescence band of the random laser was measured separately by collecting the emission at the back of the samples, showing a linear dependence with pumping fluence without gain depletion. However, frontal collection showed the saturation of emission and absorption. The emission spectrum of the peak mode (localized modes) shows approximately equal intensity, indicating suppression of the interaction between the peaks modes. The linewidth of these peaks is lower than that of the passive modes of the scattering medium, which was attributed to an anomalous nonlinear increase of the refractive index by localization.

COMPLEX LIGHT AND OPTICAL FORCES XII, Proceedings of SPIE, 10549, 105490D, 2018. DOI: 10.1117/12.2289228

[P458-2018] "Localization of light: Beginning of a new optics"

Jimenez-Villar, E.*; Xavier, M. C. S.; Ramos, J. G. G. S.; Wetter, N. U.; Mestre, V.; Martins, W. S.; Basso, G. F.; **Ermakov, V. A.*; Marques, F. C.*;** de Sa, G. F.

In recent years, there has been a dramatic progress in the photonics field of disordered media, ranging from applications in solar collectors, photocatalyzers, random lasing, and other novel photonic devices, to investigations into fundamental topics, such as localization of light and other phenomena involving photon interactions. Anderson localization of light is an open researcher frontier, which has greatly attracted the attention of researchers in the past few decades. In this work, we study the transport of light in a strongly disordered optical medium composed by core-shell nanoparticles (TiO2@Silica) suspended in ethanol solution. We demonstrate the crossover from a diffusive transport to a localization transition regime as TiO2@Silica nanoparticle concentration is increased. A striking phenomenon of enhanced absorption, mainly near the input border, arises at the localization transition, from which an increase of refractive index was inferred. An increase of the density of localized states and absorption near the input border is reported when the incidence angle is increased. The specular reflection, measured for the photons that enter the sample, is considerably lower than the effective internal reflection undergone by the coherently backscattered photons in the exact opposite direction, indicating a non-reciprocal propagation of light (parity-symmetry breaking). A theoretical simulation, performed through random-matrix theory, agrees satisfactorily with the experimental results, showing the generality of this approach to address transport phenomena.

COMPLEX LIGHT AND OPTICAL FORCES XII , Proceedings of SPIE, 10549, 1054905, 2018. DOI: 10.1117/12.2288993

[P459-2018] "Photonic molecules for application in silicon--on-insulator optical sensors"

Barea, L. A. M.; **Souza, M. C. M. M.*; Moras, A. L.***; Catellan, A. R. G.; Cirino, G. A.; **Von Zuben, A. A. G.***; Bassani, J. W. M. ; **Frateschi, N. C.***

Optical sensors based on integrated photonics have experienced impressive advancements in the past few decades and represent one of the main sensing solutions in many areas including environmental sensing and medical diagnostics. In this context, optical microcavities are extensively employed as refractive index (RI) sensors, providing sharp optical resonances that allow the detection of very small variations in the surrounding RI. With increased sensitivity, however, the device is subjected to environmental perturbations that can also change the RI, such as temperature variations, and therefore compromise their reliability. In this work, we present the concept and experimental realization of a photonic sensor based on coupled microcavities or Photonic Molecules (PM) in which only one cavity is exposed to the sensing solution, allowing a differential measurement of the RI change. The device consists of an exposed 5-mu m radius microdisk resonator coupled to an external clad microring resonator fabricated on silicon-on-insulator (SOI) platform. This design allows good sensitivity (26 nm/RIU) for transverse electrical mode (TE-mode) in a compact footprint (40 x 40 mu m(2)), representing a good solution for real-life applications in which measurement conditions are not easily controllable.

SILICON PHOTONICS XIII, Proceedings of SPIE, 10537, 105371B, 2018. DOI: 10.1117/12.2287844

Correções

[Co006-2018] "Dynamical system analysis of interacting models (vol 50, 1, 2018)"

Carneiro, S.*; Borges, H. A.

Unfortunately, there are typos in Equations (20) and (22), as well as in the line following equation (27).

GENERAL RELATIVITY AND GRAVITATION 50[10], 129, 2018. DOI: 10.1007/s10714-018-2458-1

Artigos aceitos para publicação

[A001-2018] "Self-tearing and self-peeling of folded graphene nanoribbons"

Fonseca, A. F.*; Galvão, D. S.*

A recent experimental study showed that an induced folded flap of graphene can spontaneously drive itself its tearing and peeling off a substrate, thus producing long, micrometer sized, regular trapezoidal-shaped folded graphene nanoribbons. As long as the size of the graphene flaps is above a threshold value, the "tug of war" between the forces of adhesion of graphene-graphene and graphene-substrate, flexural strain of folded region and carbon-carbon (CC) covalent bonds favor the self-tearing and self-peeling off process. As the detailed information regarding the atomic scale mechanism involved in the process remains not fully understood, we carried out atomistic reactive molecular dynamics simulations to address some features of the process. We show that large thermal fluctuations can prevent the process by increasing the probability of chemical reactions between carbon dangling bonds of adjacent graphene layers. The effects of the strength of attraction between graphene and the substrate on the ribbon growth velocities at the early stages of the phenomenon were also investigated. Structures with initial armchair crack-edges were observed to form more uniform cuts than those having initial zigzag ones. Our results are of importance to help set up new experiments on this phenomenon, especially with samples with nanoscale sized cuts.

Carbon 143, 230-239, March 2019. DOI: 10.1016/j.carbon.2018.11.020

***Autores da comunidade IFGW**
Fonte: Web of Science on-line (WOS)

Defesas de Dissertações do IFGW

[D018-2018] "Modelos análogos para os espaços-tempos de Schwarzschild e Reissner-Nordstrom"
Aluno: Christyan Costa de Oliveira
Orientador: Prof. Dr. Ricardo Antonio Mosna
Data: 30/11/2018

[D019-2018] "Estudo sobre as Flutuações Induzidas por Banhos Térmicos Finitos"
Aluno: Arthur Mendonça Faria
Orientador: Prof. Dr. Marcus Vinicius Segantini Bonança
Data: 17/12/2018

[D020-2018] "Co-dopagem por EU e Tb em Nitreto de Silício Amorfo"
Aluno: Diego Silva de Oliveira
Orientador: Prof. Dr. Leandro Russovski Tessler
Data: 19/12/2018

Defesas de Teses do IFGW

[T018-2018] "Fibras ópticas especiais para sensoriamento"
Aluno: Giancarlo Chesini
Orientador: Prof. Dr. Cristiano Monteiro de Barros Cordeiro
Data: 04/12/2018

[T019-2018] "Caracterização físico-química, estudo das propriedades de adsorção e da atividade fotocatalítica de nanocristais de diamante, nitreto de carbono grafítico e suas heterojunções"
Aluno: Julio Alberto Peres Ferencz Júnior
Orientador: Prof. Dr. Luiz Fernando Zagonel
Data: 10/12/2018

Fonte: Portal IFGW/Pós-graduação - Agenda de Colóquios, Defesas e Seminários.
Disponível em: http://portal.ifi.unicamp.br/pos-graduacao

Defesas de Dissertações e Teses do PECIM (orientadores do IFGW)

[Pe004-2018] QUALIFICAÇÃO: "CONTRIBUIÇÕES PARA A EDUCAÇÃO: O ENEM COMO INDICADOR FORMATIVO PARA O ENSINO DE FÍSICA"
Aluno: Guilherme Stecca Marcom
Orientador: Prof. Dr. Mauricio Urban Kleinke
Data: 28/11/2018
Doutorado

[Pe005-2018] QUALIFICAÇÃO: "A influência do status socioeconômico no desempenho dos estudantes nos itens de Física do Enem"
Aluno: Giuliano Perina Spazziani
Orientador: Prof. Dr. Mauricio Urban Kleinke
Data: 07/12/2018
Mestrado

Fonte: Página do PECIM - Programa de Pós-Graduação Multiunidades em Ensino de Ciências e Matemática – Mestrado e Doutorado (PECIM) da Unicamp.
Disponível em: https://www.pecim.unicamp.br/bancas

A Equipe da BIF deseja a todos Boas Festas!

Abstracta

Instituto de Física
Diretor: Prof. Dr. Pascoal José Giglio Pagliuso
Diretora Associada: Profa. Dra. Mônica Alonso Cotta
Universidade Estadual de Campinas - UNICAMP
Cidade Universitária Zeferino Vaz
13083-859 - Campinas - SP - Brasil
e-mail: secdir@ifi.unicamp.br
Fone: +55 19 3521-5300

Publicação

Biblioteca do Instituto de Física Gleb Wataghin
http://portal.ifi.unicamp.br/biblioteca

Diretora Técnica: Sandra Maria Carlos Cartaxo
Coordenadora da Comissão de Biblioteca: Profa. Dra. Arlene Cristina Aguilar

Elaboração:
Maria Graciele Trevisan (Bibliotecária)
Arthur Antunes Araujo (Estagiário)
contato: infobif@ifi.unicamp.br